Journal Pre-proofs

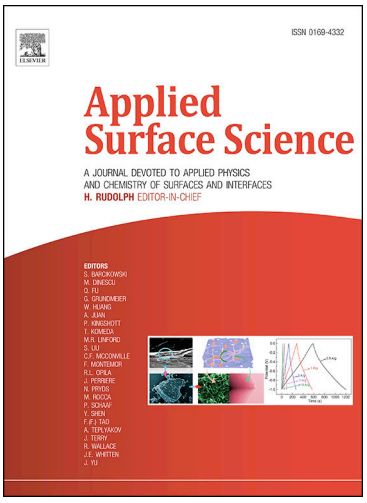

Full Length Article

New findings regarding the role of copper entity particle size on the performance of Cu/ceria-based catalysts in the CO-PROX reaction

J.C. Martínez-Munuera, J. Giménez-Mañogil, M.P. Yeste, A.B. Hungría, M.A. Cauqui, A. García-García, J.J. Calvino

PII: S0169-4332(21)02761-6
DOI: https://doi.org/10.1016/j.apsusc.2021.151717
Reference: APSUSC 151717

To appear in: *Applied Surface Science*

Received Date: 29 August 2021
Revised Date: 13 October 2021
Accepted Date: 22 October 2021

Please cite this article as: J.C. Martínez-Munuera, J. Giménez-Mañogil, M.P. Yeste, A.B. Hungría, M.A. Cauqui, A. García-García, J.J. Calvino, New findings regarding the role of copper entity particle size on the performance of Cu/ceria-based catalysts in the CO-PROX reaction, *Applied Surface Science* (2021), doi: https://doi.org/10.1016/j.apsusc.2021.151717

New findings regarding the role of copper entity particle size on the performance of Cu/ceria-based catalysts in the CO-PROX reaction

J.C. Martínez-Munuera[a], J. Giménez-Mañogil[a], M.P. Yeste[b*], A.B. Hungría[b], M.A. Cauqui[b], A. García-García[a*], J.J. Calvino[b]

[a]*MCMA Group, Department of Inorganic Chemistry and Institute of Materials, University of Alicante, Carretera San Vicente del Raspeig s/n, 03690 San Vicente del Raspeig-Alicante, Spain*

[b]*Grupo de Química de Sólidos y Catálisis, Dpto. de Ciencia de los Materiales e Ingeniería Metalúrgica y Química Inorgánica e Instituto Universitario de Investigación en Microscopía Electrónica y Materiales, Universidad de Cádiz, Puerto Real, Spain*

Abstract

The preferential oxidation of CO in H_2-rich mixtures has been studied using $Ce_{0.8}Zr_{0.2}O_2$-supported Cu catalysts containing increasing amounts of copper [1 wt% (Cu1/CZ), 2 wt% (Cu2/CZ) and 4 wt% (Cu4/CZ)]. The oxide support was prepared by co-precipitation and the copper was incorporated using the wetness impregnation method. The catalysts were characterized using N_2 adsorption, XRD, STEM-XEDS, H_2-TPR, H_2 chemisorption and XPS techniques. In particular, the complementarity of electron microscopy and hydrogen chemisorption techniques was found to be very useful for elucidating one of the most challenging properties of copper catalysts, namely their dispersion. The results show that the Cu1/CZ catalyst is the most active in the CO-PROX reaction at low temperatures (<125°C), despite having a lower copper content. The results are discussed and correlated with the textural properties of the catalysts and with parameters such as metal dispersion and the binary interfacial active sites.

Keywords: Copper-ceria-zirconia; CO-PROX; STEM-XEDS; copper dispersion; H_2 chemisorption

**Corresponding author (1). Tel.: +34 956012022; e-mail: pili.yeste@uca.es*

**Corresponding author (2). Tel.: +34 965909419; e-mail: a.garcia@ua.es*

1. Introduction

It has recently become increasingly important to search for more efficient and cleaner routes of energy production, especially as regards environmental protection, with fuel cells being seen as a promising technology in this regard. Among them, proton exchange membrane fuel cells (PEMFCs) are considered to be the most promising as they are capable of operating in both stationary and mobile devices [1–3].

Although these cells are well developed, some improvements, such us the use of a CO-free fuel stream so that the platinum electro-catalysts are not poisoned, are still needed before they can be used commercially. The preferential oxidation of CO in H_2-rich gas mixtures generated during reforming processes (CO-PROX) is a good option in this regards as it provides a fuel with a high hydrogen concentration [4,5]. In the CO-PROX process, the oxidation of carbon monoxide to carbon dioxide occurs in a mixture of carbon monoxide, oxygen and hydrogen. As such, a catalyst should be found that can oxidise carbon monoxide instead of hydrogen, which would result in a waste of fuel, although other types of reactions can also occur. [5].

Although noble metals are very active in the oxidation of CO [6–8] and yield quite robust catalysts for the PROX reaction [9], they present a number of disadvantages. The most important ones are that they are scarce resources with very high price and highly fluctuant. To overcome these limitations, Cu/Ce-based CO-PROX catalysts have attracted increasing interest recently because of their high activity and selectivity in this process, wide temperature window of operation as well as their low price compared to their noble metal-based counterparts [10–13].

A great deal of effort has gone into determining the source of the superior performance of Cu/Ce-based catalysts in CO-PROX. However, the exact origin of this enhanced catalytic activity is still unclear. According to the literature [14,15], the activity of CuO-CeO_2 catalysts improves with increasing dispersion of the copper species, probably due to the formation of oxygen vacancies at the Cu-Ce boundary which favours the reduction of copper species [16,17]. Thus, Manzoli et al. [18] have reported that the activity of Cu-CeZr catalysts at low temperature is more closely related to copper sites in close contact with CeO_2 than copper sites in interaction with ZrO_2. Similarly, the activity of copper entities has been found to depend on the dispersion as well as the degree of interaction with cerium. [16,19] In a related study, Guo et al. [20] prepared Cu-Ce catalysts with different copper contents and found that the catalytic activity was correlated with higher copper dispersion, although they do not evaluate copper dispersion in a direct manner.

Although all the previous literature points to the key role of the structure of cerium-based copper catalysts in PROX, there are very few studies in which copper dispersion has been directly and correctly determined [21–27]. Thus, in most studies, copper dispersion is only evaluated by XRD [28–30]. For example, Wang et. al [28] prepared two Cu-CeZr catalysts using two different methods, namely urea grind combustion and impregnation, and found that the sample prepared by urea grind combustion presented the best activity. In the XRD spectrum, the peaks corresponding to Cu species were only observed in the sample prepared by impregnation, which was interpreted as an indication of a lower copper dispersion. Other, more recent studies have proposed N_2O chemisorption analysis of pre-reduced catalysts under H_2 to determine the copper dispersion and corresponding average particle size.[31] However, there is an inherent drawback in this type of measurements, namely that because of the high activity of oxygen vacancies formed

during the pre-reduction, N_2O could be reoxidised on these vacancies (yielding N_2), which would lead to an overestimation of the copper dispersion.

In other studies, the catalytic behaviour in the CO-PROX reaction has been related to the amount of Cu^+ species [32–35]. This is the case, for example, for a study in which Cu-CeO_2 catalysts were produced using a solvent-free combustion synthesis.[33] However, the dispersion of copper was not measured in any of these studies. In summary, although all these studies have highlighted the synergistic effect between copper and ceria on catalytic activity, the origin of the performance of these catalysts, and particularly the influence of Cu particle size on PROX, is still unclear.

To take a further step towards clarifying this question, the aim of this work is to provide a better understanding of the relationship between the catalytic and structural/chemical properties of Cu-CeZr catalysts for CO-PROX, specifically as regards the role of copper dispersion. In this regard, it should be noted that state-of-the-art analytical studies based on aberration-corrected scanning transmission electron microscopy, particularly X-ray energy dispersive spectroscopy (STEM-XEDS), now allow a detailed compositional analysis of materials with atomic resolution. Moreover, the high sensitivity of new multidetector systems provides the means to detect even very small concentrations of a large variety of elements. Taking advantage of these instrumental advancements and given the differences in the XEDS fingerprints of Ce and Cu, whose X-ray emission peaks do not overlap on the energy scale, high resolution mapping of Cu opens the door to a direct visualization of very small nanostructures, as will be shown here. This possibility, which is beyond the reach of other transmission (TEM) or scanning-transmission electron microscopy (STEM) techniques, due to their intrinsic contrast generation mechanisms, provides the basis for an unbiased, quantitative and reliable estimation of Cu dispersion.

This is clearly novel and differential contribution of this study when compared with all the previous literature on this topic.

Three catalysts with increasing amounts of copper were prepared and characterized using a combination of macroscopic and microscopic techniques (BET analysis, XRD, STEM-XEDS, XPS, H_2-TPR). Consecutive H_2 chemisorption isotherms at different temperatures were used to determine average copper dispersion values, and the results were subsequently compared with those obtained from detailed nanoscopic studies (STEM-XEDS). In parallel, the catalytic performance of the selected catalysts in the CO-PROX reaction was evaluated. An attempt was then made to establish a structure–activity relationship based on all the structural and physicochemical characterization studies.

2. Experimental

2.1 Catalyst preparation

The $Ce_{0.8}Zr_{0.2}O_2$ (CZ) support was prepared by a co-precipitation method using $(NH_4)_2Ce(NO_3)_6$ and $ZrO(NO_3)_2{\times}H_2O$ as precursors, mixing them in de-ionized water until neutral pH. The precipitates were obtained by adding a 10 wt% NH_3 solution until pH 9. After washing and filtering, the solid was dried at 110 °C in an oven for 12 hours and then calcined in air (500 °C 1 h). Cu-CZ catalysts with Cu concentrations of 1, 2 and 4 wt% (denoted as Cu1/CZ, Cu2/CZ and Cu4/CZ respectively) were prepared using $Cu(NO_3)_2{\cdot}3H_2O$ with different concentrations as precursor. After each impregnation cycle, the samples were dried for 12 hours and finally calcined in air (500 °C 1 h). More details can be found elsewhere [36]. Table 1 shows nominal copper content and measured values obtained by X-Ray Fluorescence spectroscopy. The measured and the nominal values are similar due to the procedure of preparation is incipient wetness impregnation and there is no loss of active phase.

2.2 Catalyst characterization

2.2.1 XRF analysis

The copper concentration was measured by X-Ray Fluorescence spectroscopy (XRF) with a Philips Magix Pro equipment (PW2400). For the analysis, the software used was SuperQ.

2.2.2. BET analysis

The surface area, as calculated using the Brunauer-Emmett-Teller (BET) method, and the pore structure, as calculated using the Barrett-Joynerr-Halenda (BJH) model, were determined from N_2 adsorption-desorption isotherms performed at -196 °C (Autosorb-6B from Quantachrome). All samples were degassed at 250 °C for 4 h.

2.2.3. XRD analysis

X-ray diffraction (XRD) patterns were recorded using a Bruker D8 diffractometer. The conditions of the study were the following: CuKα radiation, 2θ angle from 10° to 60°.

2.2.4. TEM analysis

High-angle annular dark field scanning transmission electron microscopy (HAADF-STEM) images and X-ray energy dispersive spectroscopy (XEDS) maps with high resolution were obtained using a double aberration-corrected FEI Titan3 Themis 60–300 microscope equipped with a four-detector ChemiStem system. A very stable stage with minimised sample drift and a sub-angstrom electron probe were used for this purpose. To sample sufficiently wide catalyst areas, large element maps (512 x 512 pixels) were acquired. The total acquisition time was 25 minutes per map. Electron microscopy

samples were prepared by depositing small portions of the catalyst powders onto a holey carbon-coated gold grid.

2.2.5. H_2-TPR analysis

Catalysts were studied by H_2-temperature programmed reduction (H_2-TPR). The analysis was performed using a Micromeritics Pulse device. The sample (20 mg) was preoxidised under O_2 (5%)/He, subsequently heating to 500 °C at 10 °C/min and then at 500 °C for 1 h. The gas was then switched to H_2(5%)/Ar and analysis was performed from room temperature to 1000 °C.

2.2.6. XPS

X-ray photoelectron spectra (XPS) were acquired using a Kα spectrometer with a charge compensation of electrons and ions. The spectra were recorded at room temperature using monochromatised Al Kα radiation (1486.6 eV) under a vacuum of 5×10^{-9} mbar. To support the analysis of the results, a CuO sample was also studied. This sample was prepared from $Cu(NO_3)_2 \cdot 3H_2O$ by calcination (500 °C, 1 h).

2.2.7. H_2 chemisorption

Chemisorption measurements were carried out using a Micromeritics ASAP 2020c device. Prior to analysis the samples were reduced in H_2(5%)/Ar at 350 °C for 1 h and then evacuated at 500 °C. Adsorption isotherms were measured at different temperatures. Two sequential isotherms were carried out at each temperature, with an evacuation under high vacuum between them. The difference between both isotherms can be ascribed to the irreversible contribution of H_2 adsorption. H_2 chemisorption measurements were performed at H_2 partial pressures ranging from 50 to 300 Torr, and seven equilibrium pressure data values were acquired.

2.3 Catalytic tests

The preferential oxidation of CO was performed at atmospheric pressure using 50 mg of catalyst with 100 mg of SiC. A gas mixture consisting of 1% CO, 1% O_2, 50% H_2 and 48% He was used at a flow rate of 100 ml/min. Prior to analysis, the catalysts were cleaned in O_2 (5%)/He at a flow rate of 60 ml/min and 500 °C (1 h). A gas chromatograph (Bruker 450-GC) was used to analyse both inlet and outlet gases. The CO conversion, O_2 conversion and selectivity (%) for CO_2 were obtained as described below:

$$CO\ conversion\ (\%) = \frac{(CO)_{in} - (CO)_{out}}{(CO)_{in}} \times 100$$

$$O_2\ conversion\ (\%) = \frac{(O_2)_{in} - (O_2)_{out}}{(O_2)_{in}} \times 100$$

$$CO_2\ Selectivity\ (\%) = \frac{CO\ conversion}{2 \times O_2\ conversion} \times 100$$

3. Results and discussion

3.3.1. BET

The physicochemical properties of the catalysts are reported in **Table 1**. It can be seen that the BET surface area of the CZ support is larger than that of the catalysts. Moreover, compared with CZ, the specific pore volumes of Cu2/CZ and Cu4/CZ have decreased significantly. These results suggest the occurrence of pore blocking upon incorporation of copper on the surface of the CZ support, although this does not appear to be proportional to copper loading. The corresponding N_2 adsorption-desorption isotherms are provided in **Figure 1A.** The catalysts show type IV isothermal curves, which are characteristic of mesoporous materials. The BJH plots (**Figure 1B**) reveal an average pore

size of close to 4 nm for all catalysts. The analysis of the textural properties yields better results for Cu1/CZ, which therefore more closely resembles the support than Cu2/CZ and Cu4/CZ.

<near Figure 1>

<near Table 1>

3.3.2. XRD

XRD diagrams for the different catalysts are shown in **Figure 2**. In all cases, the peaks are attributable to the cubic structure of CeO_2 (JCPDS 34-0394). The characteristic peaks appears at higher diffraction angles with respect to those of the reference CeO_2 phase, thus reflecting the lattice contraction due to the introduction of zirconium into the fluorite network of the cerium oxide ($r(Ce^{4+}) = 0.097$ nm versus $r(Zr^{4+}) = 0.084$ nm) [37,38]. The additional diffraction peaks observed in the Cu4/CZ pattern (35.5° and 38.7°) correspond to the monoclinic structure of CuO (JCPDS48-1548). This implies that, in this catalyst, and due to the higher copper loading, CuO is not as well dispersed, as observed in a previous study [39], and that the tenorite phase is detectable. Diffraction peaks for the tenorite phase are not observed for the other catalysts, thus suggesting that CuO is highly dispersed on the support [40], which is in good agreement with the TEM results (see below). The lattice parameters and crystal sizes estimated using PowderCell23 software [41] are shown in **Table 1**. The lattice values are very similar, thus suggesting that copper is not integrated into the CeZr network.

<near Figure 2>

3.3.3. TEM

High-resolution HAADF-STEM images were acquired to characterize the copper oxide in the catalysts (**Figure 3**). Since the intensity of HAADF-STEM images is proportional to the square of the atomic number of the element, the low atomic number of Cu compared to Ce and Zr makes the difference in contrast between the oxidised copper phase and the mixed cerium-zirconium oxide very low in these images, thus meaning that the nanoparticles of the copper phase could not be identified.

In order to locate and characterize the copper nanoparticles, STEM-XEDS maps were recorded in different parts of the sample. In these maps, a full XEDS spectrum is recorded on each pixel of the acquired image, thus allowing the different elements present in the location corresponding to that pixel to be detected.

Figures 3 a), **c)** and **e)** show HAADF-STEM images for three representative areas of the Cu1/CZ, Cu2/CZ and Cu4/CZ catalysts where XEDS maps were acquired, (**Figures 3 b**), **d)** and **f)**, respectively). It can be observed, first of all, that cerium and zirconium are distributed homogeneously in the support for all samples, as expected. Similarly, copper is clearly detected in the form of very small particles, with an average size of 0.9 and 1.1 nm for Cu1/CZ and Cu2/CZ, respectively. However, the particle-size distribution seems to be very narrow for Cu1/CZ and relatively broad for Cu2CZ, as also reflected in the corresponding histograms included in Figure S1 of the Supplementary Information. This is in agreement with the dispersion values for Cu1/CZ (74%) and Cu2/CZ (60%) calculated using the Rhodius program [42].

The situation for Cu4/CZ is different. Thus, for this catalyst, aggregates of copper-containing particles with a size of about 100 nm were found throughout the regions analysed. Some areas with small copper oxide particles were also found, as shown in Figure S2 in the SI, although the areas with large particles (see **Figures 3e**) and **3f**)) reduce down the average metal dispersion in this sample.

<near Figure 3>

3.3.4. H_2-TPR analysis

The TPR experiments for the different catalysts, together with those for the reference oxides, are shown in **Figure 4**. Note that the CZ support displays one very broad peak in the 450–650°C range. This feature is commonly ascribed to reduction of the surface and a fraction of the bulk oxygens in the mixed ceria-zirconia oxide [43]. CuO reduction proceeds with a single peak centred at 350°C. In the case of Cu/CZ catalysts, the TPR plots show two distinct reduction events followed by an extremely broad reduction at higher temperatures. The two major peaks appear at roughly 160 and 280°C, i.e. clearly shifted towards lower temperatures with respect to the individual components (CZ and CuO). These shifts prove the occurrence of an interaction between Cu and Ce. This enhancement in copper reduction due to ceria has already been reported in the literature [33,434,45]. Thus, the low-temperature peak has tentatively been related to the reduction of highly dispersed CuO, while the highest temperature one has been associated with the reduction of large CuO particles [39]. However, other authors indicate that the appearance of two different peaks is due to the initial reduction of Cu^{2+} to Cu^{+}, followed by reduction of the latter to Cu^{0}. In any case, the larger the CuO particles, the higher the reduction temperature [46].

The second peak in the reduction profile of Cu4/CZ is shifted to higher temperatures with respect to those of Cu1/CZ and Cu2/CZ. This would agree well with the former hypothesis, and the second reduction event could be ascribed to transformation of the hundreds of nanometre-sized, bulk-like CuO particles detected in the Cu4/CZ catalyst in both the XRD and STEM-XEDS maps. Nevertheless, to clarify the involvement of the different reducible species in the two major reduction events, a quantitative analysis of the H_2-TPR signals was performed (**Table 2**). The results clearly indicate that, for all

catalysts, hydrogen consumption is much higher than that which would have been expected for the full reduction of all the CuO content of the catalysts given that, considering the well-assumed stoichiometry, the H_2/CuO molar ratio should be 1. This fact suggests that a higher number of neighbouring cerium centres per mol of copper are affected for the catalyst with the lowest copper content. This is in agreement with the higher copper dispersion and narrow particle-size distribution determined for Cu1/CZ. These determinations suggest that copper promotes reduction of the cerium centres by H_2 to a greater degree, as has already been observed for supported noble metals [47–49], and that the degree and extent of reduction of the cerium centres is influenced by copper dispersion. Indirectly, this could suggest the highest "effectiveness" of the Cu/CeZr interphase for Cu1CZ (binary interfacial active sites), since a higher number of cerium centres in the proximity of Cu species can be reduced by H_2 (due to spillover phenomena) when compared with Cu2/CZ and Cu4/CZ.

<near Figure 4>

<near Table 2>

3.3.5. XPS

The catalysts were analysed by XPS to provide information regarding the oxidation states of copper, since Cu^+ has been proposed to be the active species for CO oxidation in some studies [22,50]. The spectrum for the reference CuO sample (**Figure 5**) contains a broad and asymmetric main $Cu2p_{3/2}$ peak centred at BE $\cong$ 933.7 eV. According to Martínez-Arias et al [51], this broad peak may be due to the contribution of different copper species. The $Cu2p_{3/2}$ signal also exhibits satellite peaks at 941.3 and 943.7 eV. In copper-containing samples, there is a satellite peak (Cu-2p spectra) due to the presence of Cu^{2+}, whereas no satellite is produced by Cu^+ and Cu^0. [45]. As a result, the relative proportion

of Cu^{2+} can be determined from the ratio of areas for the satellite peak (A_{sat}) and the main Cu-$2p_{3/2}$ peak (A_{mp}), taking bulk CuO, which exhibits a ratio of 0.5 (A_{sat}/A_{mp}), as reference. [49]. The ratios for the catalysts studied are shown in Table 3. It can be seen that the results differ markedly from 0.50 for the samples with a low copper content (1% and 2%) but are closer to 0.50 for Cu4/CZ. It is important to bear in mind that, for this last sample, evidence for a CuO phase was obtained by XRD, as well as the presence of aggregates of copper-containing particles about 100 nm in size in some of the regions analysed by STEM-XEDS. However, the other catalysts studied have a low A_{sat}/A_{mp} value, which suggests the coexistence of Cu^{2+} and Cu^{+} and could be linked to the higher degree of dispersion of the copper-containing particles found in these catalysts. Nevertheless, the attribution is not completely conclusive due to the difficulty of copper species' oxidation states identification as well pointed out in previous related works [36,52,53].

In addition, the surface atomic composition was studied by XPS. The Cu/(Cu+Ce+Zr) surface ratios were compared to the bulk atomic ratios (**Table 3**) and a higher copper enrichment on the particles' surface was found for Cu4/CZ, exceedingly probably, the capacity of support dispersion. Similarly, CuO_x aggregates entities were identified by the previous techniques discussed. In contrast, the closest match among surface and bulk Cu/(Cu+Ce+Zr) values found for Cu1/CZ would suggest a very good distribution of copper species, which is consistent with the best dispersion values and very narrow particle-size distribution found for Cu1/CZ.

<near Figure 5>

<near Table 3>

3.3.6. H_2 adsorption volumetric studies

According to the literature, hydrogen spillover observed in hydrogen adsorption experiments on ceria/zirconia-supported noble-metal catalysts also takes place in Cu/ceria-zirconia systems [50,54]. As such, estimation of the irreversible H_2 chemisorption capacity of the catalysts in volumetric experiments carried out at sub-ambient temperature has proved to be the best approach to obtain reliable metal dispersion data for the catalyst. [55]. However, the activated nature of hydrogen chemisorption on copper [56] precludes the use of this experimental procedure in Cu/ceria-zirconia catalysts. In this case, under sub-ambient conditions, adsorption would lead to hydrogen coverages that would underestimate the fraction of surface-exposed metallic sites. Consequently, H_2 chemisorption isotherms at temperatures ranging from 50 to 150°C were recorded in our studies (**Figure 6A**). The fraction corresponding to strong, irreversible H_2 chemisorption on copper was estimated from the difference between the isotherms corresponding to total and weakly reversible H_2 chemisorption. In particular, extrapolation of the difference isotherm to zero pressure was used as a measure of the hydrogen chemisorption capacity on copper in the different catalysts. **Figure 6A** shows the results for Cu2/CZ as a representative example. Note how a decrease in irreversible H_2 uptake takes place after increasing the adsorption temperature from 50 to 100°C. However, a further increase of temperature up to 150°C leads to a decrease in H_2 uptake. These results suggest that the monolayer coverage is reached when adsorption experiments are carried out at 100°C. Taking this into account, the monolayer coverage for all catalysts was estimated at 100°C in the chemisorption experiments (**Figure 6B**).

Apart from the influence of hydrogen-spillover phenomena, the determination of copper dispersion values from supposedly pure chemisorption on Cu centres is further complicated by the fact that different H/Cu chemisorption stoichiometries may occur [57]. Thus, if a 1:1 H/Cu chemisorption stoichiometry is assumed, Cu1/CZ would be the

catalyst with the highest copper dispersion (71%), followed by Cu2/CZ (57%), whereas Cu4/CZ exhibits a much lower dispersion value (35%) than Cu1/CZ. These results confirm, at a macroscopic level, the values obtained from the STEM-XEDS study (74% for Cu1/CZ and 60% for Cu2/CZ) and indicate an interesting similarity between particle sizes determined for very small CuO_x species well-dispersed on the support, which are very difficult to determine for ceria-zirconia, using two different techniques. Thus, advanced microscopy techniques and a relatively simple procedure based on H_2 chemisorption volumetric studies (conducted using much more accessible equipment), both of which provided average values for copper dispersion at a macroscopic level, give very similar results.

<near Figure 6>

3.3.7. Catalytic activity in the PROX reaction

Given the good understanding of the physicochemical features of the catalysts under investigation, they were studied in the CO-PROX reaction in an attempt to correlate their properties with catalytic performance. Since the behaviour of these catalysts has been proved in other oxidation reactions of environmental interest (NO oxidation, diesel soot combustion, CO oxidation under different atmospheres [36,58], etc.), a combined discussion will be presented in this section to shed some light on the reasons for their different catalytic activities and to detect any correlations with the physicochemical features of the solids.

Figure 7 shows the activity results after a pre-conditioning treatment. **Figure 7A** depicts the CO conversion, **Figure 7B** the O_2 conversion and, finally, **Figure 7C** the selectivity towards CO_2 as reaction product. The maximum data error was ±1.5 %. The estimated carbon balances were always in the range 97% - 103%. Therefore, within the error of

determination of the components. All three catalysts exhibit a high CO conversion and selectivity towards CO_2, even outperforming the values reported in the recent literature [40,59]. It should be highlighted that Cu1/CZ displays a CO conversion of 20% at 50°C (onset reaction temperature), with a selectivity of 100%. In general, the different profiles (**Figures 7A**, **B**, **C**) present the expected shape for the CO-PROX reaction conditions used given the competing reactions occurring (CO oxidation versus H_2 oxidation reaction). As a result, upon increasing the temperature, H_2 oxidation gains relevance and gradually hinders CO oxidation because of the thermodynamic values (ΔH^0) of the H_2 oxidation (-242 KJ/mol) and CO oxidation (-283 HJ/mol). ~~limited O_2 supply~~, Thereby eventually causing a decrease in CO conversion at 175 or 200°C (depending on the catalyst's formulation; see **Figure 7A**).

In the present work, the copper-containing catalysts exhibit a slight decrease in BET surface area with the increase in metal loading due to partial blocking of porosity as a consequence of the incipient wetness impregnation procedure used. In order to determine the extent of the influence of this decrease on the catalytic activity, **Figure 8** illustrates specific rates for this set of catalysts normalized to catalyst surface area. Surface-area normalized values were derived from the rate of CO conversion per second and per square meter of solids' surface areas. By comparing the interval of low temperatures of Fig. 7A with that of Fig. 8, it can be said that the trends are very similar, thus suggesting that the concentration of active sites per m^2 seems to be larger for Cu1/CZ. This supports the idea that the highest BET surface area of this sample is not the only factor affecting the goodness of Cu1/CZ and the reason why this catalyst has the maximum activity per gram (Fig. 7A) is not only due to its highest surface area.

Following in this line, it results relevant to compare the activity per exposed surface atom in the form of turnover frequency (TOF). Values normalised to number of exposed copper

atoms were determined experimentally (by using the data of copper dispersion). The corresponding representation of TOF in terms of temperature is reflected in **Figure 9**. TOF values follow the order Cu1/CZ>>Cu2/CZ>Cu4CZ. This could imply that the better copper dispersion data as the copper loading decreases provides a better "quality" of the binary interfacial sites (Cu-Ce) as well. If cerium centres of these interfaces are reduced under reaction conditions, then concomitant oxygen vacancies creation (as active sites) will play a role. However, due to the presence of 1%O_2 in the reaction stream, all the active species able to take part in the reaction could be eventually re-oxidised and reduced, in subsequent steps. All these features make complex a deeper discussion on identification of active sites under *operando* conditions. Nevertheless, the experimental results presented so far provide strong evidences of the relevant role of copper entities' dispersion accompanied by the population of binary interfacial sites as a direct consequence of this very high metallic dispersion. All these features joined to the trend of BET surface areas for the three catalysts, becomes higher and higher the differences in the samples, being the best catalytic behaviour that shown by Cu1/CZ.

Conversely, the trend in catalytic activity at low temperatures as a function of copper loading observed for the PROx reaction (Fig. 7A) is not that noted for related reactions involving CO reaction atmospheres (CO oxidation under anaerobic conditions and CO oxidation under O_2 presence), the corresponding profiles for which can be seen in Figures S3 and S4, respectively, for comparison purposes. Under these reaction conditions, Cu1/CZ presents the lowest activity, whereas Cu2/CZ and Cu4/CZ appear to exhibit similar abilities to activate CO molecules (Cu4/CZ being slightly more active than Cu2/CZ) and oxidise them using lattice oxygen (which is eventually replaced by gas-phase O_2), according to the well-accepted Mars-van-Krevelen mechanism for these reactions. Other reported catalytic results related to other oxidation reactions of

environmental interest (e.g. NO oxidation under O_2) yielded similar trends, as reported by other authors [36]. This supports the trends noted for the selected catalysts, which are the same (under CO or NO) in the absence of a H_2-reducing atmosphere.

The results presented so far reveal that the dispersion of copper entities on ceria-zirconia is not the only key factor that accounts for the order in catalytic activities and that the activity order observed for CO-PROX reactions is not that found for CO oxidation without H_2, or for other common oxidation reactions.

Although, Martínez-Arias et al. reported detailed *operando* studies that highlighted the key role of copper oxidation states [60–63], there is still some debate regarding the competitive nature of CO and H_2 oxidation reactions. Thus, the presence of a large excess of H_2 in the reaction atmosphere might condition the surface chemistry of the selected catalysts during these processes. As a result, the CO-PROX process is rather complex and the nature of the active sites probably differs from that existing and prevailing in the absence of H_2. Assuming that CO and H_2 oxidation are activated at different active sites [10] (CO oxidation may be favoured at stable and active surface Cu^+ species balanced in several CuO environments, whereas H_2 oxidation is likely to take place extensively when metallic copper entities are formed as a result of the presence of H_2), the highest copper dispersion found for Cu1/CZ (together with the very narrow particle-size distribution) may favour the reduction of CuO_x entities to Cu^+ species in the early stages of the reaction and therefore play a key role. As the reaction proceeds and large-scale reduction of Cu^+ to metallic copper occurs for Cu1/CZ, the selectivity for CO_2 drops markedly, in the range 75-150°C, compared with that observed for Cu2/CZ and Cu4/CZ (**Figure 7C**). Above 150°C, all three catalysts are seen to converge to the same CO conversion and CO_2 selectivity profiles. A tentative explanation for this may be that, by this stage, all three have reached similar degrees of copper reduction under *operando* conditions (despite

having different copper loadings, dispersion values and textural properties). This is not found, however, for the other CO oxidation reactions, (Fig, S3 and S4), and at 150°C, the CO oxidation curves for Cu1/CZ (expressed as CO_2 concentration) are still below those for Cu2/CZ and Cu4/CZ.

It is important to remember that Cu1/CZ was found to have the highest BET surface area and total pore volume and the best "extra" reducibility under H_2 (expressed as H_2/CuO molar ratio; see **Table 2**). As such, the delicate balance exhibited by the Cu1/CZ catalyst in terms of copper entity dispersion, which in turn seems to originate a better "quality" of the interfacial sites, (Fig. 9) and their accessibility to the reactive atmosphere, makes this catalyst more active in the CO-PROX reaction than the other two, which have higher copper contents and exhibit a higher activity in CO oxidation reactions in the absence of additional reducing atmospheres.

Finally, the results presented herein may lead to a better understanding of the role of copper/ceria-based catalysts under these conditions and provide new insights for the rational design of competitive catalysts in the future.

<near Figure 7>

<near Figure 8>

<near Figure 9>

4. Conclusions

Copper-ceria-zirconia catalysts with different Cu loadings (1, 2 and 4 wt%) have been prepared, characterized and evaluated in the CO-PROX reaction. The use of STEM-XEDS with multidetector systems has allowed us to directly visualize small copper nanostructures and determine the Cu particle-size distribution with much higher accuracy.

This is one of the key findings of this study compared with previous studies. The dispersion data determined by STEM-XEDS were found to be in good agreement with those obtained by hydrogen chemisorption studies at 100°C.

The results presented reveal that copper dispersion is a very important factor, but not the only one explaining the order of catalytic activity. Thus, in CO-PROX, the catalyst with the highest dispersion (Cu1/CZ) is the most active at low temperature (<125°C). The highest dispersion of this catalyst may favour the reduction of CuO_x entities to Cu^+/Cu^0 during the course of the reaction. Moreover, in addition to better dispersion data, this catalyst exhibits a high quality of the Cu-Ce interface and better textural properties. These facts make Cu1/CZ a more active catalyst in the CO-PROX reaction than the other catalysts analysed despite their higher copper contents.

CRediT authorship contribution statement

J.C. Martínez-Munuera: Investigation. J. Giménez-Mañogil: Investigation. M.P. Yeste: Investigation, Writing - Original Draft. A.B. Hungría: Investigatio. M.A. Cauqui: Writing - Review & Editing. A. García-García: Writing - Original Draft, Supervision. J.J. Calvino: Writing - review & editing.

Acknowledgements

The authors gratefully acknowledge financial support from the Generalitat Valenciana (PROMETEO/2018/076 project), the Spanish Ministry of Science and Innovation (PID2019-105542RB-I00 and MAT2017-87579-R projects) and UE-FEDER. J.C. Martínez-Munuera also acknowledges the Spanish Ministry of Science and Innovation for financial support through an FPU grant (FPU17/00603).

4. References

[1] A. Biyikoğlu, Review of proton exchange membrane fuel cell models, Int. J. Hydrogen Energy. 30 (2005) 1181–1212. doi:10.1016/j.ijhydene.2005.05.010.

[2] M.J. Escudero, M.P. Yeste, M.A. Cauqui, M.A. Muñoz, Performance of a Direct Methane Solid Oxide Fuel Cell Using Nickel-Ceria-Yttria Stabilized Zirconia as the Anode, Materials (Basel). 13 (2020) 599. doi:10.3390/ma13030599.

[3] K. Vidal, A. Larrañaga, A. Morán-Ruiz, A.T. Aguayo, M.A. Laguna-Bercero, M.P. Yeste, J.J. Calvino, M.I. Arriortua, Effect of synthesis conditions on electrical and catalytical properties of perovskites with high value of A-site cation size mismatch, Int. J. Hydrogen Energy. 41 (2016) 19810–19818. doi:10.1016/j.ijhydene.2016.02.088.

[4] A.F. Ghenciu, Review of fuel processing catalysts for hydrogen production in PEM fuel cell systems, Curr. Opin. Solid State Mater. Sci. 6 (2002) 389–399. doi:10.1016/S1359-0286(02)00108-0.

[5] E.D. Park, D. Lee, H.C. Lee, Recent progress in selective CO removal in a H_2-rich stream, Catal. Today. 139 (2009) 280–290. doi:10.1016/j.cattod.2008.06.027.

[6] M.J. Kahlich, H.A. Gasteiger, R.J. Behm, Kinetics of the selective CO oxidation in H_2-rich gas on Pt/Al_2O_3, J. Catal. 171 (1997) 93–105. doi:10.1006/jcat.1997.1781.

[7] C. Galletti, S. Specchia, G. Saracco, V. Specchia, Catalytic performance of rhodium-based catalysts for CO preferential oxidation in H_2-rich gases, Ind. Eng. Chem. Res. 47 (2008) 5304–5312. doi:10.1021/ie0713588.

[8] J.L. Ayastuy, M.P. González-Marcos, J.R. González-Velasco, M.A. Gutiérrez-Ortiz, $MnOx/Pt/Al_2O_3$ catalysts for CO oxidation in H_2-rich streams, Appl. Catal.

B Environ. 70 (2007) 532–541. doi:10.1016/j.apcatb.2006.01.028.

[9] L. Cao, W. Liu, Q. Luo, R. Yin, B. Wang, J. Weissenrieder, M. Soldemo, H. Yan, Y. Lin, Z. Sun, C. Ma, W. Zhang, S. Chen, H. Wang, Q. Guan, T. Yao, S. Wei, J. Yang, J. Lu, Atomically dispersed iron hydroxide anchored on Pt for preferential oxidation of CO in H2, Nature. 565 (2019) 631-635.

doi:10.1038/s41586-018-0869-5.

[10] A. Martínez-Arias, D. Gamarra, A.B. Hungría, M. Fernández-García, G. Munuera, A. Hornés, P. Bera, J.C. Conesa, A.L. Cámara, Characterization of Active Sites/Entities and Redox/Catalytic Correlations in Copper-Ceria-Based Catalysts for Preferential Oxidation of CO in H_2-Rich Streams, Catalysts. 3 (2013) 378–400. doi:10.3390/catal3020378.

[11] J.L. Ayastuy, A. Gurbani, M.P. González-Marcos, M.A. Gutiérrez-Ortiz, Effect of copper loading on copper-ceria catalysts performance in CO selective oxidation for fuel cell applications, Int. J. Hydrogen Energy. 35 (2010) 1232–1244. doi:10.1016/j.ijhydene.2009.11.098.

[12] F. Mariño, C. Descorme, D. Duprez, Supported base metal catalysts for the preferential oxidation of carbon monoxide in the presence of excess hydrogen (PROX), Appl. Catal. B Environ. 58 (2005) 175–183. doi:10.1016/j.apcatb.2004.12.008.

[13] M.P. Yeste, H. Vidal, A.L. García-Cabeza, J.C. Hernández-Garrido, F.M. Guerra, G.A. Cifredo, J.M. González-Leal, J.M. Gatica, Low temperature prepared copper-iron mixed oxides for the selective CO oxidation in the presence of hydrogen, Appl. Catal. A Gen. 552 (2018) 58–69. doi:10.1016/j.apcata.2017.12.012.

[14] D. Gamarra, A. Hornés, Z. Koppány, Z. Schay, G. Munuera, J. Soria, A. Martínez-Arias, Catalytic processes during preferential oxidation of CO in H_2-rich streams over catalysts based on copper-ceria, J. Power Sources. 169 (2007) 110–116. doi:10.1016/j.jpowsour.2007.01.048.

[15] D.H. Kim, J.E. Cha, A CuO-CeO2 mixed-oxide catalyst for CO clean-up by selective oxidation in hydrogen-rich mixtures, Catal. Letters. 86 (2003) 107–112. doi:10.1023/A:1022671327794.

[16] A. Martínez-Arias, A.B. Hungría, M. Fernández-García, J.C. Conesa, G. Munuera, Preferential oxidation of CO in a H2-rich stream over CuO/CeO2 and CuO/(Ce,M)Ox (M = Zr, Tb) catalysts, in: J. Power Sources, Elsevier, 2005: pp. 32–42. doi:10.1016/j.jpowsour.2005.02.078.

[17] P. Ratnasamy, D. Srinivas, C.V.V. Satyanarayana, P. Manikandan, R.S. Senthil Kumaran, M. Sachin, V.N. Shetti, Influence of the support on the preferential oxidation of CO in hydrogen-rich steam reformates over the CuO-CeO_2-ZrO_2 system, J. Catal. 221 (2004) 455–465. doi:10.1016/j.jcat.2003.09.006.

[18] M. Manzoli, R. Di Monte, F. Boccuzzi, S. Coluccia, J. Kašpar, CO oxidation over CuOx-CeO_2-ZrO_2 catalysts: Transient behaviour and role of copper clusters in contact with ceria, Appl. Catal. B Environ. 61 (2005) 192–205. doi:10.1016/j.apcatb.2005.05.005.

[19] A. Martínez-Arias, J. Soria, R. Cataluña, J.C. Conesa, V. Certés Corberán, Influence of ceria dispersion on the catalytic performance of Cu/(CeO_2)/Al_2O_3 catalysts for the CO oxidation reaction, Stud. Surf. Sci. Catal. 116 (1998) 591–600. doi:10.1016/s0167-2991(98)80914-2.

[20] X. Guo, J. Mao, R. Zhou, Influence of the copper coverage on the dispersion of

copper oxide and the catalytic performance of CuO/CeO2(rod) catalysts in preferential oxidation of CO in excess hydrogen, J. Power Sources. 371 (2017) 119–128. doi:10.1016/j.jpowsour.2017.10.055.

[21] A. Davó-Quiñonero, M. Navlani-García, D. Lozano-Castelló, A. Bueno-López, J.A. Anderson, Role of Hydroxyl Groups in the Preferential Oxidation of CO over Copper Oxide-Cerium Oxide Catalysts, ACS Catal. 6 (2016) 1723–1731. doi:10.1021/acscatal.5b02741.

[22] E. Moretti, M. Lenarda, P. Riello, L. Storaro, A. Talon, R. Frattini, A. Reyes-Carmona, A. Jiménez-López, E. Rodríguez-Castellón, Influence of synthesis parameters on the performance of CeO_2-CuO and CeO_2-ZrO_2-CuO systems in the catalytic oxidation of CO in excess of hydrogen, Appl. Catal. B Environ. 129 (2013) 556–565. doi:10.1016/j.apcatb.2012.10.009.

[23] J.S. Moura, J.D.S.L. Fonseca, N. Bion, F. Epron, T.D.F. Silva, C.G. Maciel, J.M. Assaf, M.D.C. Rangel, Effect of lanthanum on the properties of copper, cerium and zirconium catalysts for preferential oxidation of carbon monoxide, Catal. Today, Elsevier, 2014: pp. 40–50. doi:10.1016/j.cattod.2013.11.016.

[24] J.L. Ayastuy, A. Gurbani, M.P. González-Marcos, M.A. Gutiérrez-Ortiz, Selective CO oxidation in H 2 streams on CuO/CexZr$_{1-x}O_2$ catalysts: Correlation between activity and low temperature reducibility, in: Int. J. Hydrogen Energy, Pergamon, 2012: pp. 1993–2006. doi:10.1016/j.ijhydene.2011.04.178.

[25] J. Oh, J. Do Yoo, K. Kim, H.J. Yun, W.C. Jung, J. Bae, Negative Effects of Dopants on Copper–Ceria Catalysts for CO Preferential Oxidation Under the Presence of CO_2 and H_2O, Catal. Letters. 147 (2017) 2987–3003. doi:10.1007/s10562-017-2188-0.

[26] C.G. MacIel, M.N. Belgacem, J.M. Assaf, Performance of CuO-CeO_2 catalysts with low copper content in CO preferential oxidation reaction, Catal. Letters. 141 (2011) 316–321. doi:10.1007/s10562-010-0486-x.

[27] P.S. Barbato, S. Colussi, A. Di Benedetto, G. Landi, L. Lisi, J. Llorca, A. Trovarelli, Origin of High Activity and Selectivity of CuO/CeO_2 Catalysts Prepared by Solution Combustion Synthesis in CO-PROX Reaction, J. Phys. Chem. C. 120 (2016) 13039–13048. doi:10.1021/acs.jpcc.6b02433.

[28] J. Wang, L. Deng, D. He, J. Lu, S. He, S. He, Y. Luo, A facile and rapid route to synthesize CuOx/$Ce_{0.8}Zr_{0.2}O_2$ catalysts with high performance for CO preferential oxidation (CO-PROX), Int. J. Hydrogen Energy. 40 (2015) 12478–12488. doi:10.1016/j.ijhydene.2015.07.063.

[29] E. Moretti, L. Storaro, A. Talon, P. Riello, A.I. Molina, E. Rodríguez-Castellón, 3-D flower like Ce-Zr-Cu mixed oxide systems in the CO preferential oxidation (CO-PROX): Effect of catalyst composition, Appl. Catal. B Environ. 168–169 (2015) 385–395. doi:10.1016/j.apcatb.2014.12.032.

[30] J. Wang, C. Han, X. Gao, J. Lu, G. Wan, D. He, R. Chen, K. Chen, S. He, Y. Luo, Rapid synthesis of Fe-doped CuO-$Ce_{0.8}Zr_{0.2}O_2$ catalysts for CO preferential oxidation in H_2-rich streams: Effect of iron source and the ratio of Fe/Cu, J. Power Sources. 343 (2017) 437–445. doi:10.1016/j.jpowsour.2017.01.084.

[31] M. Zabilskiy, I. Arčon, P. Djinović, E. Tchernychova, A. Pintar, In-situ XAS Study of Catalytic N_2O Decomposition Over CuO/CeO_2 Catalysts, ChemCatChem. 13 (2021) 1814–1823. doi:10.1002/cctc.202001829.

[32] A.F. Zedan, K. Polychronopoulou, A. Asif, S.Y. AlQaradawi, A.S. AlJaber, Cu-Ce-O catalyst revisited for exceptional activity at low temperature CO oxidation

reaction, Surf. Coatings Technol. 354 (2018) 313–323. doi:10.1016/j.surfcoat.2018.09.035.

[33] J. Lu, J. Wang, Q. Zou, D. He, L. Zhang, Z. Xu, S. He, Y. Luo, Unravelling the Nature of the Active Species as well as the Doping Effect over Cu/Ce-Based Catalyst for Carbon Monoxide Preferential Oxidation, ACS Catal. 9 (2019) 2177–2195. doi:10.1021/acscatal.8b04035.

[34] X. Guo, R. Zhou, Identification of the nano/micro structure of CeO2(rod) and the essential role of interfacial copper-ceria interaction in CuCe(rod) for selective oxidation of CO in H_2-rich streams, J. Power Sources. 361 (2017) 39–53. doi:10.1016/j.jpowsour.2017.06.064.

[35] K. Kappis, J. Papavasiliou, Influence of the Hydrothermal Parameters on the Physicochemical Characteristics of Cu−Ce Oxide Nanostructures, ChemCatChem. 11 (2019) 4765–4776. doi:10.1002/cctc.201901108.

[36] J. Giménez-Mañogil, A. Bueno-López, A. García-García, Preparation, characterisation and testing of $CuO/Ce_{0.8}Zr_{0.2}O_2$ catalysts for NO oxidation to NO_2 and mild temperature diesel soot combustion, Appl. Catal. B Environ. 152–153 (2014) 99–107. doi:10.1016/j.apcatb.2014.01.018.

[37] J. Deng, S. Yuan, L. Xiong, S. Li, J. Wang, Y. Chen, Synthesis and characterization of nanostructured CeO_2-ZrO_2 material with improved low-temperature reducibility, Mater. Charact. 155 (2019) 109808. doi:10.1016/j.matchar.2019.109808.

[38] E. Mamontov, T. Egami, R. Brezny, M. Koranne, S. Tyagi, Lattice defects and oxygen storage capacity of nanocrystalline ceria and ceria-zirconia, J. Phys. Chem. B. 104 (2000) 11110–11116. doi:10.1021/jp0023011.

[39] M.P. Yeste, M.A. Cauqui, J. Giménez-Mañogil, J.C. Martínez-Munuera, M.A. Muñoz, A. García-García, Catalytic activity of Cu and Co supported on ceria-yttria-zirconia oxides for the diesel soot combustion reaction in the presence of NOx, Chem. Eng. J. 380 (2020) 122370. doi:10.1016/j.cej.2019.122370.

[40] J. Lu, J. Wang, Q. Zou, Y. Zhao, J. Fang, S. He, D. He, Y. Luo, Catalytic performance of transition metals (Co, Ni, Zn, Mo) doped CuO-$Ce_{0.8}Zr_{0.2}O_2$ based catalysts for CO preferential oxidation in H_2-rich streams, J. Alloys Compd. 784 (2019) 1248–1260. doi:10.1016/j.jallcom.2019.01.107.

[41] W. Kraus, G. Nolze, POWDER CELL - A program for the representation and manipulation of crystal structures and calculation of the resulting X-ray powder patterns, J. Appl. Crystallogr. 29 (1996) 301–303. doi:10.1107/S0021889895014920.

[42] S. Bernal, F.J. Botana, J.J. Calvino, G.A. Cifredo, J.A. Pérez-Omil, J.M. Pintado, HREM study of the behaviour of a Rh/CeO_2 catalyst under high temperature reducing and oxidizing conditions, Catal. Today. 23 (1995) 219–250. doi:10.1016/0920-5861(94)00165-X.

[43] N. Guillén-Hurtado, A. Bueno-López, A. García-García, Surface and structural characterisation of coprecipitated $Ce_xZr_{1-x}O_2$ ($0 \geq x \geq 1$) mixed oxides, J. Mater. Sci. 47 (2012) 3204–3213. doi:10.1007/s10853-011-6158-4.

[44] G. Avgouropoulos, T. Ioannides, Selective CO oxidation over CuO-CeO_2 catalysts prepared via the urea-nitrate combustion method, Appl. Catal. A Gen. 244 (2003) 155–167. doi:10.1016/S0926-860X(02)00558-6.

[45] J. Xiaoyuan, L. Guanglie, Z. Renxian, M. Jianxin, C. Yu, Z. Xiaoming, Studies of pore structure, temperature-programmed reduction performance, and micro-

structure of CuO/CeO_2 catalysts, Appl. Surf. Sci. 173 (2001) 208–220. doi:10.1016/S0169-4332(00)00897-7.

[46] M. Zabilskiy, P. Djinović, B. Erjavec, G. Dražić, A. Pintar, Small CuO clusters on CeO_2 nanospheres as active species for catalytic N_2O decomposition, Appl. Catal. B Environ. 163 (2015) 113–122. doi:10.1016/j.apcatb.2014.07.057.

[47] M. Labaki, S. Aouad, S. Hany, C. Abou Serhal, E. Abi-Aad, A. Aboukaïs, Physico-chemical investigation of catalytic oxidation sites in $4\%Rh/CeO_2$ catalysts prepared by impregnation and deposition–precipitation methods, Chem. Phys. 527 (2019) 110472. doi:10.1016/j.chemphys.2019.110472.

[48] J. Fan, Y. Chen, X. Jiang, P. Yao, Y. Jiao, J. Wang, Y. Chen, A simple and effective method to synthesize Pt/CeO2 three-way catalysts with high activity and hydrothermal stability, J. Environ. Chem. Eng. 8 (2020) 104236. doi:10.1016/j.jece.2020.104236.

[49] K. Xi, Y. Wang, K. Jiang, J. Xie, Y. Zhou, H. Lu, Support interaction of Pt/CeO_2 and Pt/SiC catalysts prepared by nano platinum colloid deposition for CO oxidation, J. Rare Earths. 38 (2020) 376–383. doi:10.1016/j.jre.2019.07.012.

[50] L. Yang, S. Zhou, T. Ding, M. Meng, Superior catalytic performance of non-stoichiometric solid solution $Ce_{1-X}Cu_xO_{2-\delta}$ supported copper catalysts used for CO preferential oxidation, Fuel Process. Technol. 124 (2014) 155–164. doi:10.1016/j.fuproc.2014.03.002.

[51] A. Martínez-Arias, M. Fernández-García, J. Soria, J.C. Conesa, Spectroscopic study of a Cu/CeO_2 catalyst subjected to redox treatments in carbon monoxide and oxygen, J. Catal. 182 (1999) 367–377. doi:10.1006/jcat.1998.2361.

[52] U. Menon, H. Poelman, V. Bliznuk, V.V. Galvita, D. Poelman, G.B. Marin, Nature of the active sites for the total oxidation of toluene by CuO-CeO_2/Al_2O_3, J. Catal. 295 (2012) 91-103.

[53] J. P. Espinós, J. Morales, A. Barranco, A. Caballero, J. P. Holgado, and A. R. González-Elipe, Interface Effects for Cu, CuO, and Cu_2O Deposited on SiO_2 and ZrO_2. XPS Determination of the Valence State of Copper in Cu/SiO_2 and Cu/ZrO_2 Catalysts, J. Phys. Chem. 106 (2002) 6921.

[54] A. Kitla, O. V. Safonova, K. Föttinger, Infrared studies on bimetallic copper/nickel catalysts supported on zirconia and ceria/zirconia, Catal. Letters. 143 (2013) 517–530. doi:10.1007/s10562-013-1001-y.

[55] J.M. Gatica, R.T. Baker, P. Fornasiero, S. Bernal, J. Kašpar, Characterization of the metal phase in NM/$Ce_{0.68}Zr_{0.32}O_2$ (NM: Pt and Pd) catalysts by hydrogen chemisorption and HRTEM microscopy: a comparative study, J. Phys. Chem. B. 105 (2001) 1191–1199. doi:10.1021/jp003632g.

[56] L. Álvarez-Falcón, F. Viñes, A. Notario-Estévez, F. Illas, On the hydrogen adsorption and dissociation on Cu surfaces and nanorows, Surf. Sci. 646 (2016) 221–229. doi:10.1016/j.susc.2015.08.005.

[57] R. Chatterjee, S. Kuld, R. van den Berg, A. Chen, W. Shen, J.M. Christensen, A.D. Jensen, J. Sehested, Mapping Support Interactions in Copper Catalysts, Top. Catal. 62 (2019) 649–659. doi:10.1007/s11244-019-01150-9.

[58] J. Giménez-Mañogil, A. García-García, Identifying the nature of the copper entities over ceria-based supports to promote diesel soot combustion: Synergistic effects, Appl. Catal. A Gen. 542 (2017) 226–239. doi:10.1016/j.apcata.2017.05.031.

[59] G.R. Kosmambetova, The Influence of Yttrium Stabilized Zirconia as Support of Copper-Ceria Systems on their Catalytic Properties in the Prox Process, Theor. Exp. Chem. 56 (2020) 346–351. doi:10.1007/s11237-020-09664-0.

[60] M. Monte, G. Munuera, D. Costa, J.C. Conesa, A. Martínez-Arias, Near-ambient XPS characterization of interfacial copper species in ceria-supported copper catalysts, Phys. Chem. Chem. Phys. 17 (2015) 29995–30004. doi:10.1039/c5cp04354a.

[61] D. Gamarra, A. López Cámara, M. Monte, S.B. Rasmussen, L.E. Chinchilla, A.B. Hungría, G. Munuera, N. Gyorffy, Z. Schay, V. Cortés Corberán, J.C. Conesa, A. Martínez-Arias, Preferential oxidation of CO in excess H_2 over CuO/CeO_2 catalysts: Characterization and performance as a function of the exposed face present in the CeO_2 support, Appl. Catal. B Environ. 130-131 (2013) 224–238. doi:10.1016/j.apcatb.2012.11.008.

[62] S. Yao, K. Mudiyanselage, W. Xu, A.C. Johnston-Peck, J.C. Hanson, T. Wu, D. Stacchiola, J.A. Rodriguez, H. Zhao, K.A. Beyer, K.W. Chapman, P.J. Chupas, A. Martínez-Arias, R. Si, T.B. Bolin, W. Liu, S.D. Senanayake, Unraveling the dynamic nature of a CuO/CeO_2 catalyst for CO oxidation in Operando: A combined study of XANES (fluorescence) and drifts, ACS Catal. 4 (2014) 1650–1661. doi:10.1021/cs500148e.

[63] J.C. Hanson, R. Si, W. Xu, S.D. Senanayake, K. Mudiyanselage, D. Stacchiola, J.A. Rodriguez, H. Zhao, K.A. Beyer, G. Jennings, K.W. Chapman, P.J. Chupas, A. Martínez-Arias, Pulsed-reactant in situ studies of ceria/CuO catalysts using simultaneous XRD, PDF and DRIFTS measurements, in: Catal. Today, Elsevier, 2014: pp. 64–71. doi:10.1016/j.cattod.2013.10.087.

Table headers.

Table 1. Copper content and main parameters obtained from textural and structural characterization of CuX/CZ catalysts and the corresponding support.

Table 2. Quantitative analysis of H_2-TPR data for Cu/CZ samples.

Table 3. XPS parameters obtained for the catalysts.

Figure captions.

Figure 1. (A) N_2 physisorption isotherms for the catalysts. The full and empty symbols correspond to adsorption and desorption branches, respectively. (B) BJH pore size distribution curves calculated from the desorption branch of the N_2 chemisorption isotherms.

Figure 2. XRD diagrams for the catalysts (JCPDS files for cubic CeO_2 and monoclinic CuO are included).

Figure 3. HAADF-STEM images together with the corresponding XEDS maps of different areas in Cu1/CZ (a and b), Cu2/CZ (c and d) and Cu4/CZ (e and f).

Figure 4. H_2-TPR profiles for the catalysts and the CuO reference sample.

Figure 5. Cu $2p_{3/2}$ photoelectron profiles for the samples studied (fitted envelope and deconvoluted peaks).

Figure 6. H_2 adsorption isotherms at different temperatures for the Cu2/CZ sample. (A) T Isotherm represents the total adsorption, R isotherms represents the reversibly adsorbed hydrogen, I (T-R) represent the irreversible adsorbed hydrogen. (B) H_2 adsorption isotherms at 100 °C for the three catalysts.

Figure 7. CO-PROX reaction curves: (A) CO conversion (%), (B) O_2 conversion (%),

(C) selectivity for CO_2 (%). Feed stream (in vol. %): $CO/O_2/H_2/He$ (1/1/50/48). Total flow rate: 100 mL/min.

Figure 8. Specific rates of CO conversion for the copper-containing catalysts.

Figure 9. TOF values as a function of temperature for the copper-containing catalysts.

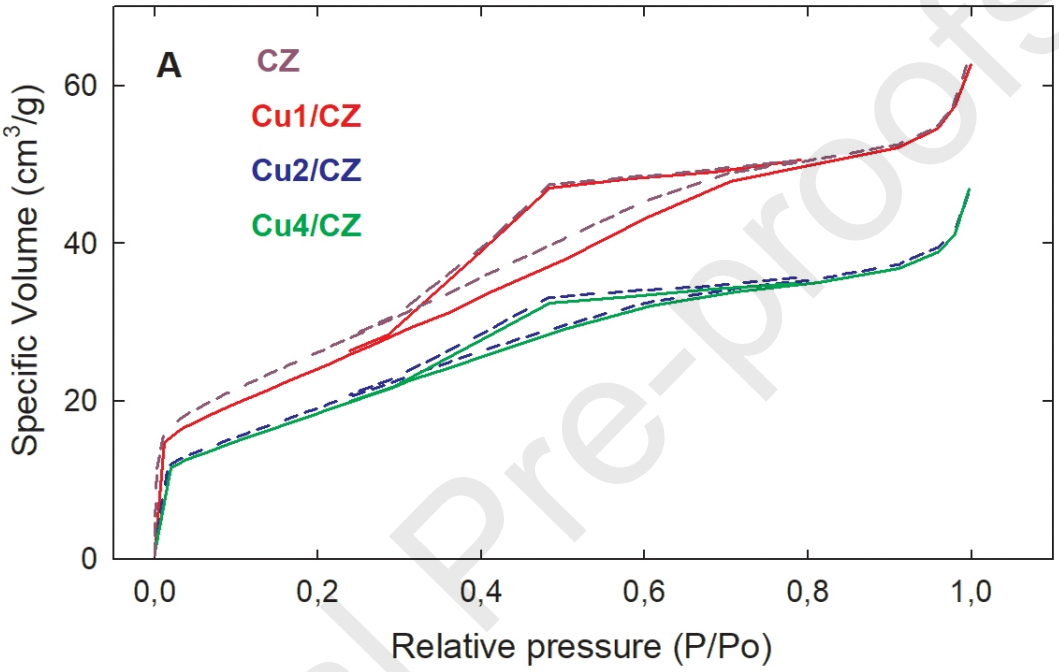

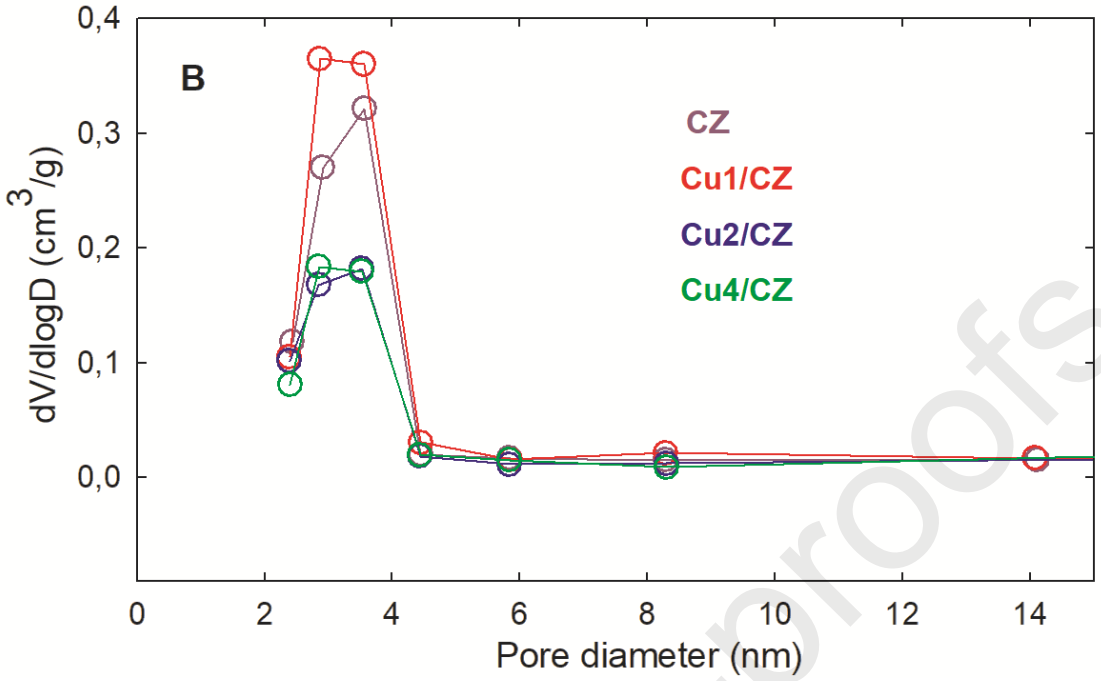

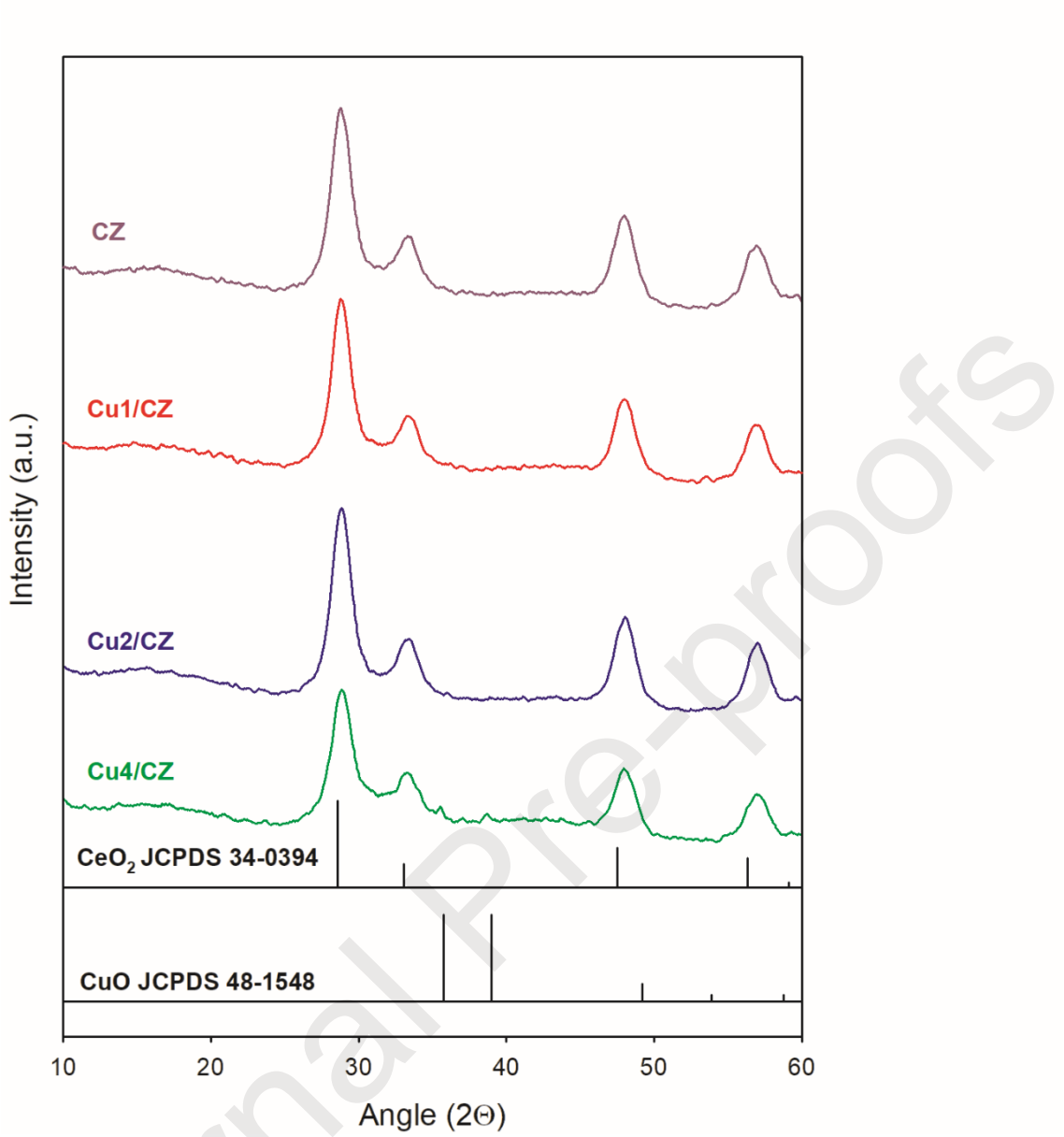

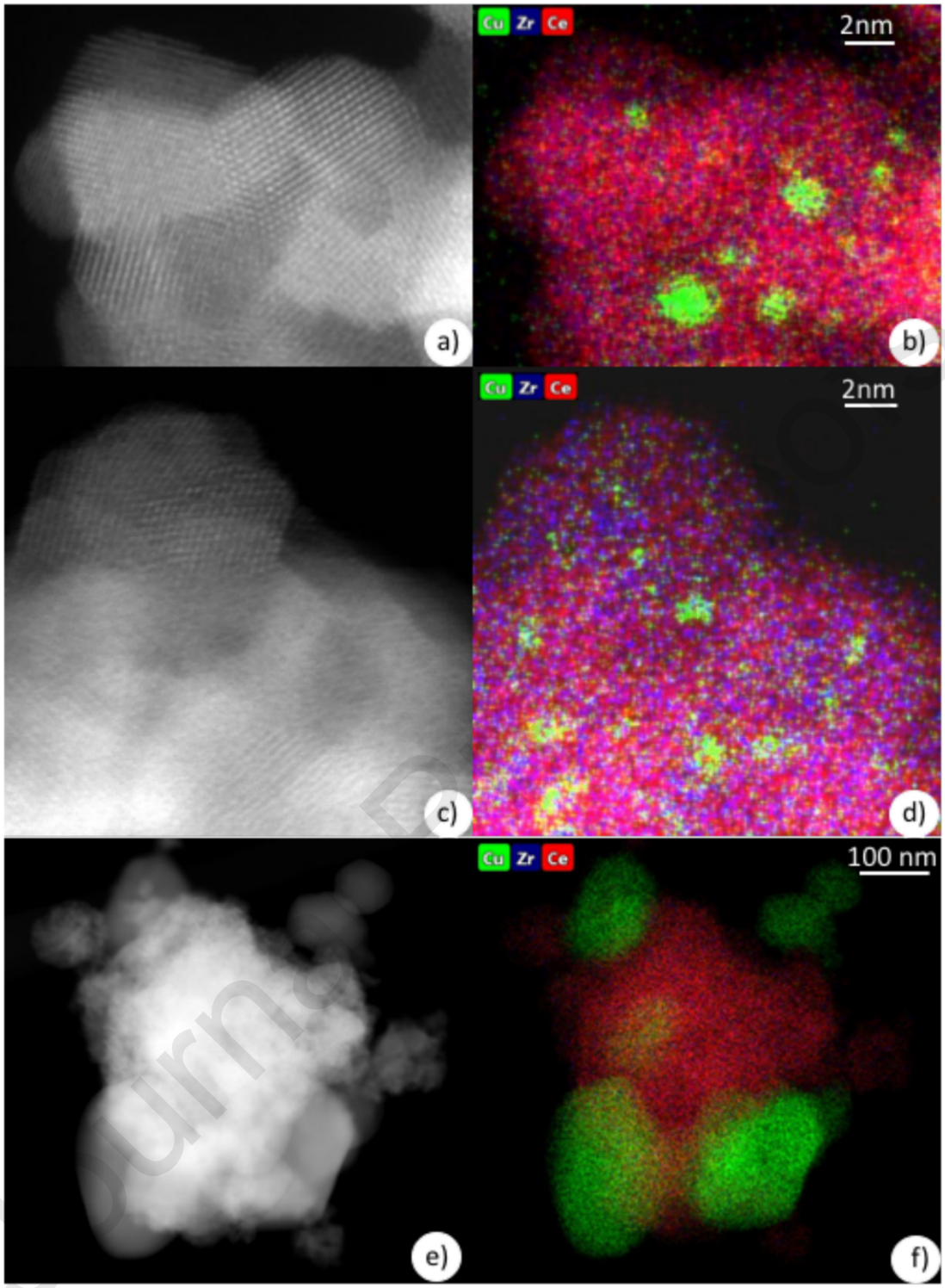
a)
Cu Zr Ce
2nm
b)
c)
Cu Zr Ce
2nm
d)
e)
Cu Zr Ce
100 nm
f)

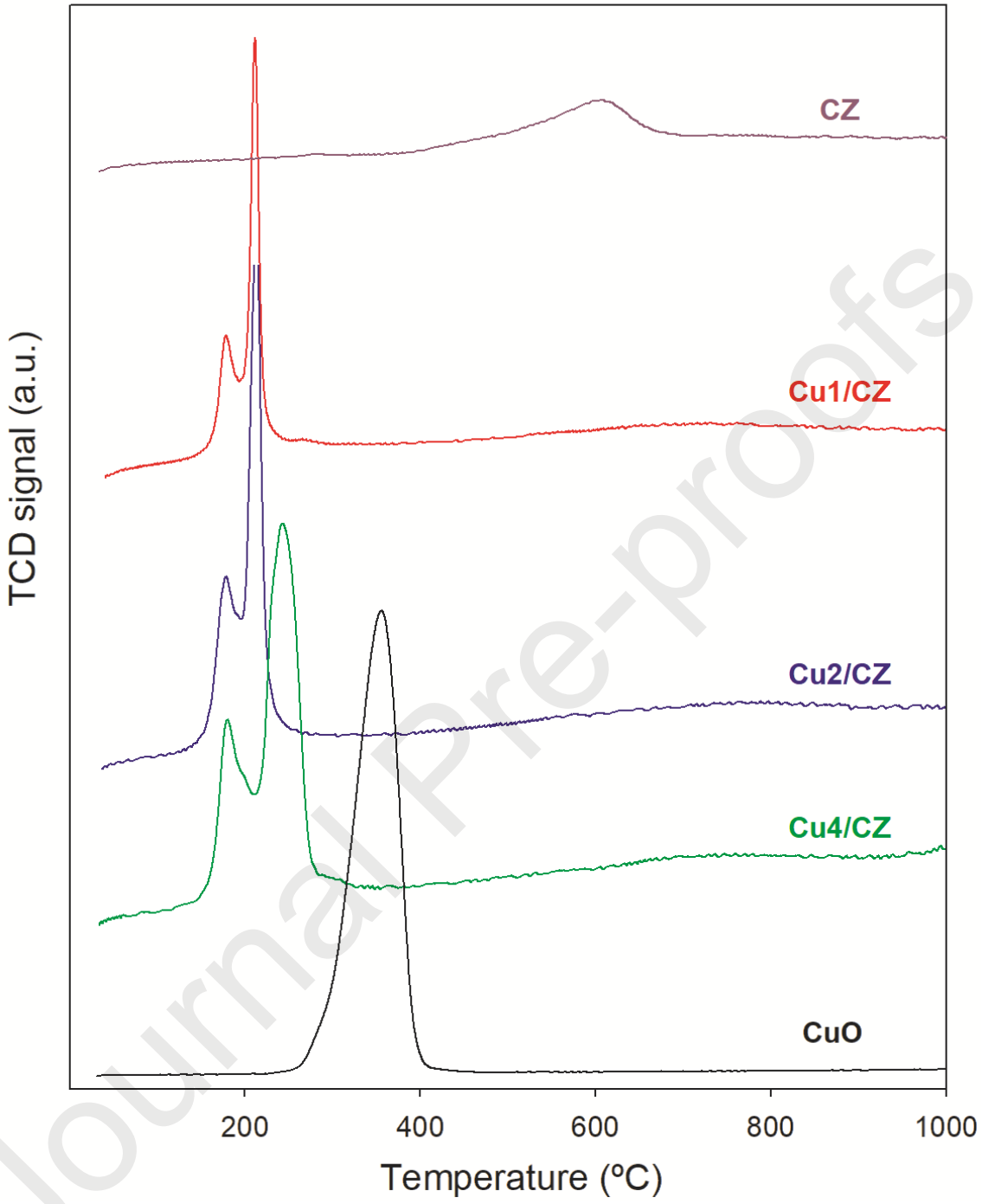

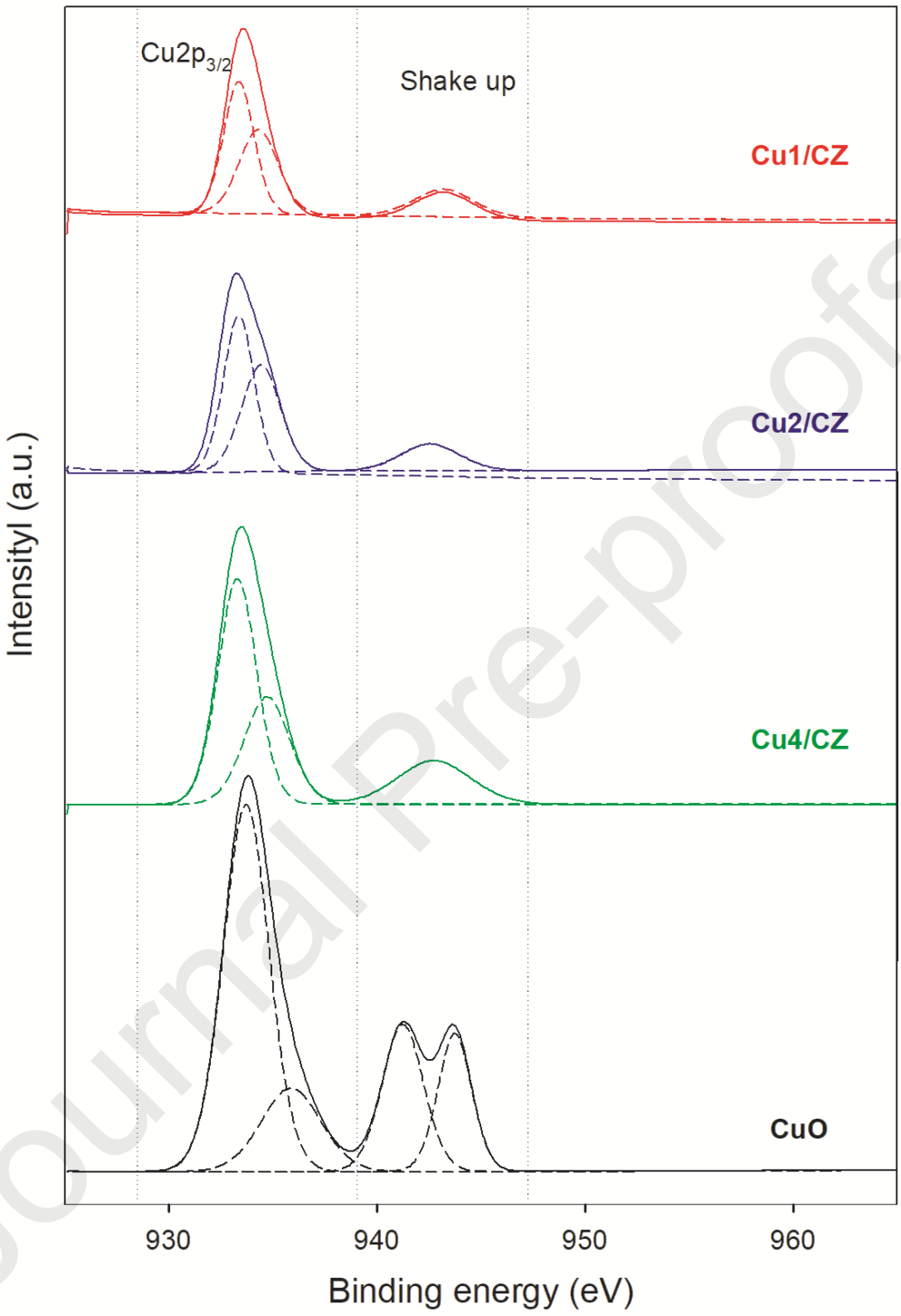

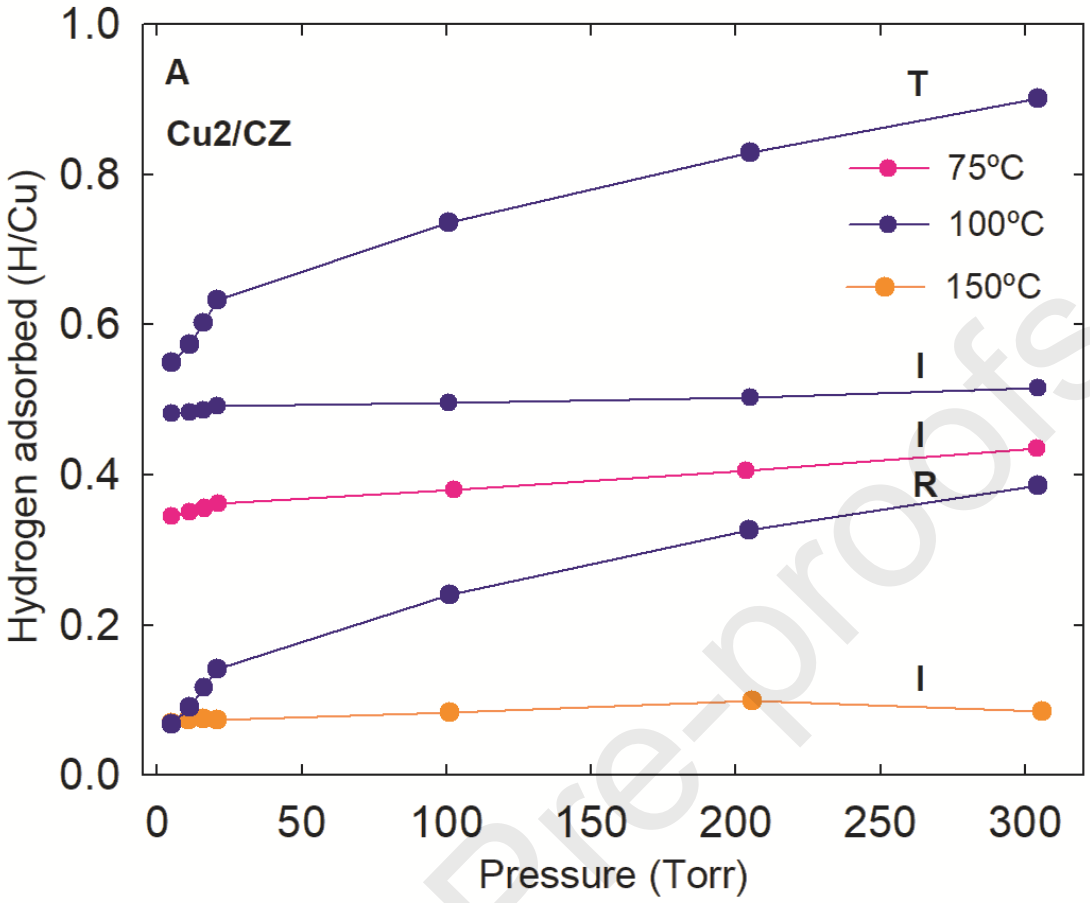

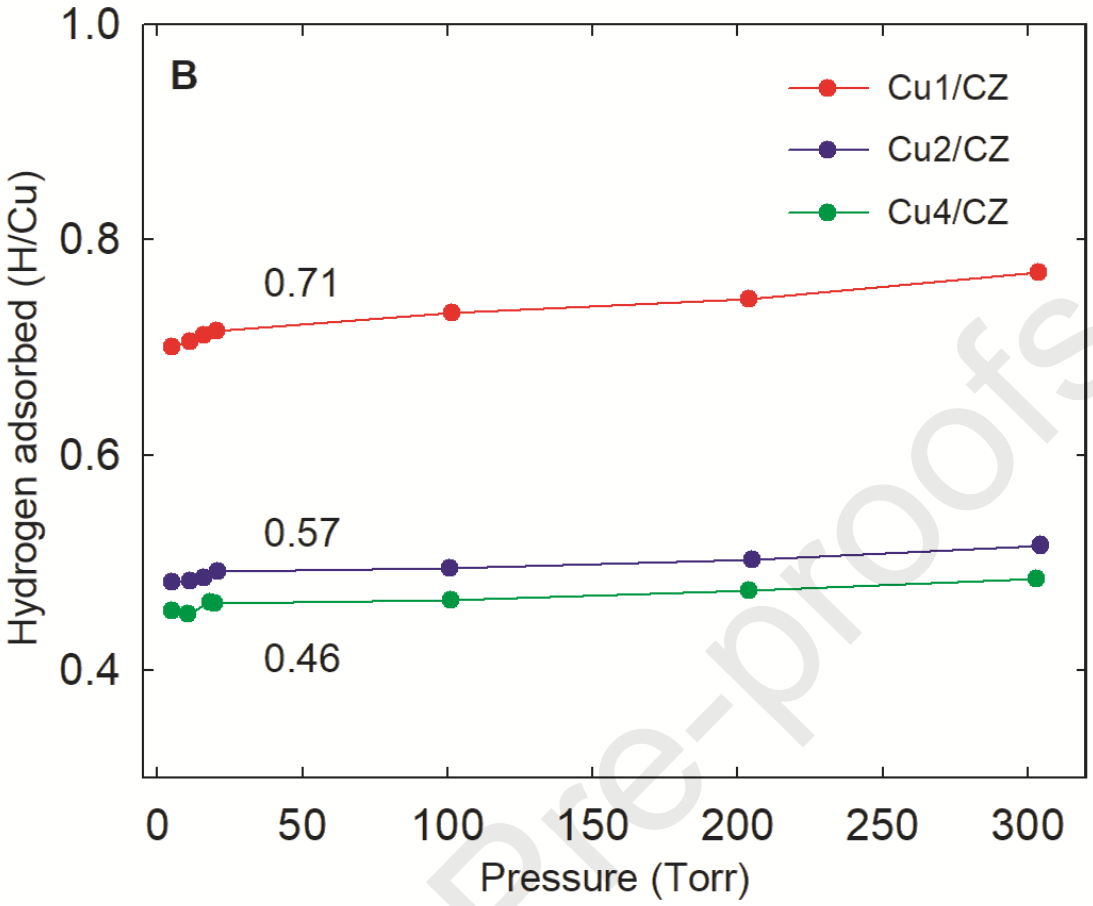

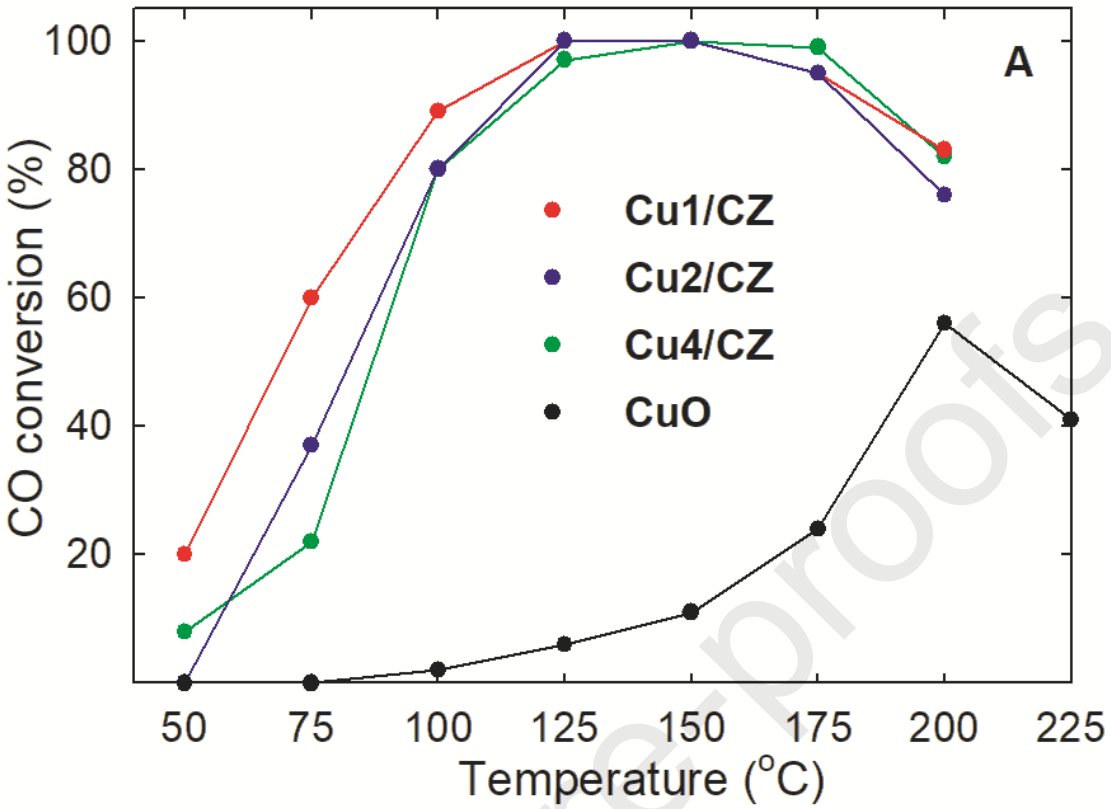

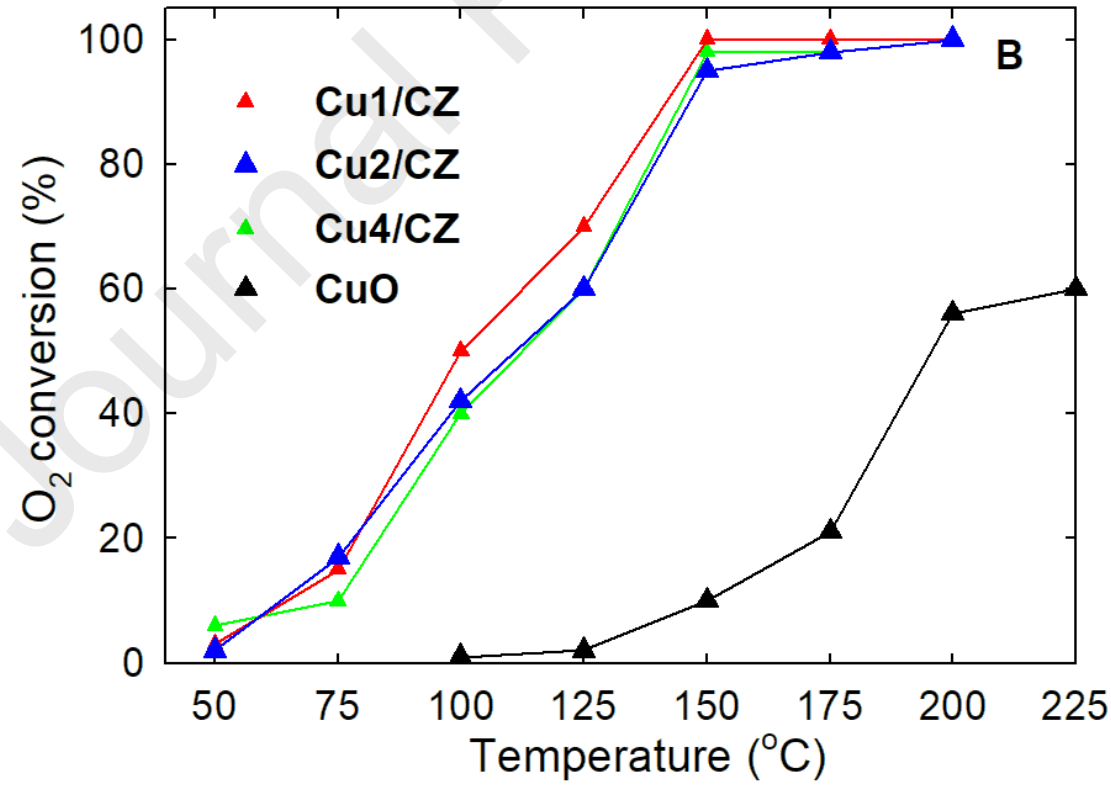

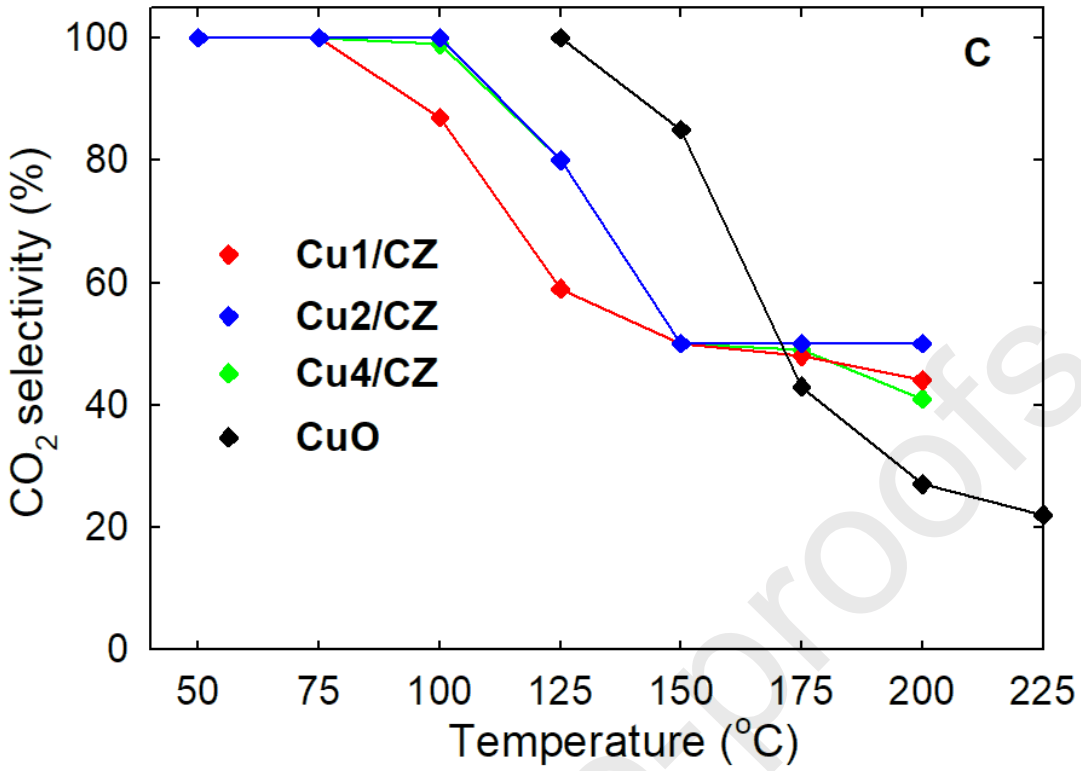

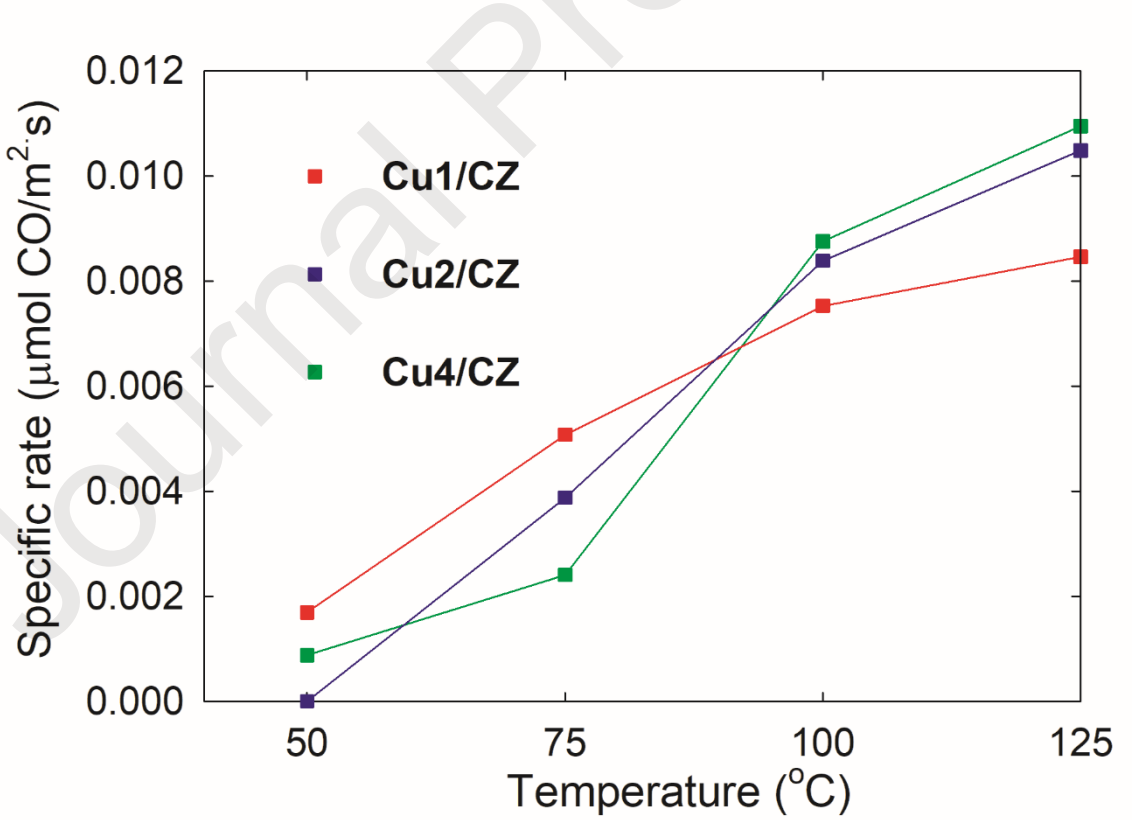

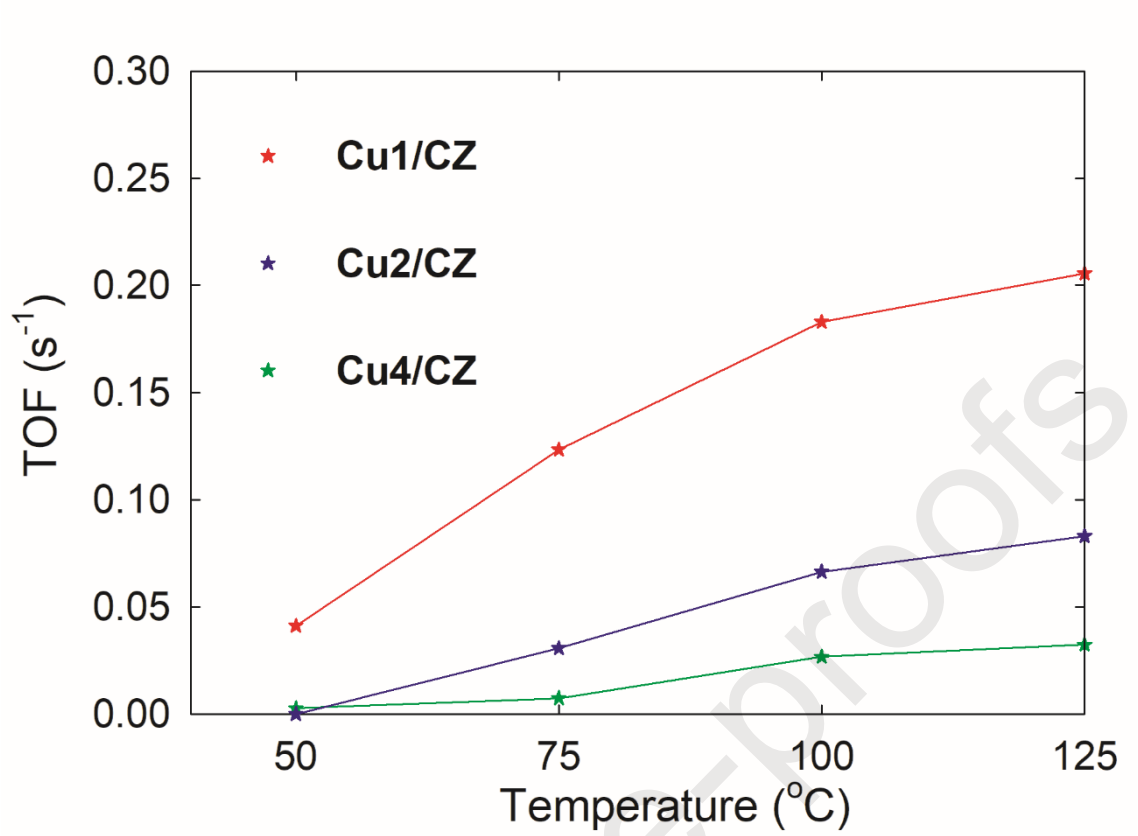

Table 1

Catalysts	Copper composition (%p/p)		S_{BET} (m^2/g)	Specific pore volume (cm^3/g)	CZ Lattice parameter (nm)	Average crystal size (nm)	
	Nominal	XRF				CZ	CuO
CZ			96	0.090	0.536	5.5	
Cu1/CZ	1.00	1.00	88	0.089	0.536	6.4	
Cu2/CZ	2.00	2.28	71	0.067	0.536	5.9	
Cu4/CZ	4.00	4.78	68	0.064	0.536	5.7	10.0

Table 2

Catalysts	Experimental H_2 consumption (µmol/g)	Theoretical CuO H_2 consumption (µmol/g)	H_2/CuO molar ratio obtained
Cu1/CZ	930	157	5.9
Cu2/CZ	1225	315	3.9
Cu4/CZ	1738	630	2.8

Table 3

Catalysts	A_{sat}/A_{mp}

	Cu/(Cu+Ce+Zr)$_{sur}$	
Cu1/CZ	0.037 (0.026)	0.22
Cu2/CZ	0.095 (0.051)	0.18
Cu4/CZ	0.282 (0.102)	0.48
CuO	--	0.50

Values in parentheses are referred to bulk or nominal atomic ratios.

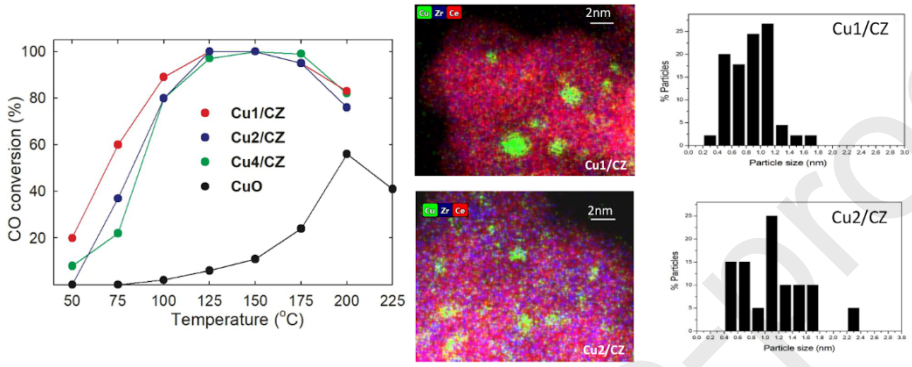

Highlights

-STEM-XEDS enables direct visualization of small copper nanostructures in catalysts.

-It is possible to measure dispersion of copper by hydrogen chemisorption at 100 ºC.

-Catalyst with high copper dispersion is the most active at low temperature in CO-PROX.

CRediT authorship contribution statement

New findings regarding the role of copper entity particle size on the performance of Cu/ceria-based catalysts in the CO-PROX reaction

J.C. Martínez-Munuera[a], J. Giménez-Mañogil[a], M.P. Yeste[b], A.B. Hungría[b], M.A, Cauqui[b], A. García-García[a]*, J.J. Calvino[b]*

[a]MCMA Group, Department of Inorganic Chemistry and Institute of Materials, University of Alicante, Carretera San Vicente del Raspeig s/n, 03690 San Vicente del Raspeig-Alicante, Spain.

[b]Grupo de Química de Sólidos y Catálisis, Dpto. de Ciencia de los Materiales e Ingeniería Metalúrgica y Química Inorgánica e Instituto Universitario de Investigación en Microscopía Electrónica y Materiales, Universidad de Cádiz, Puerto Real, Spain.

CRediT authorship contribution statement

J.C. Martínez-Munuera: Investigation. J. Giménez-Mañogil: Investigation. M.P. Yeste: Investigation, Writing - Original Draft. A.B. Hungría: Investigatio. M.A. Cauqui: Writing - Review & Editing. A. García-García: Writing - Original Draft, Supervision. J.J. Calvino: Writing - review & editing.

Correspondence to:

**E-mail address corresponding author (1): pili.yeste@uca.es*

**E-mail address corresponding author (2): a.garcia@ua.es*

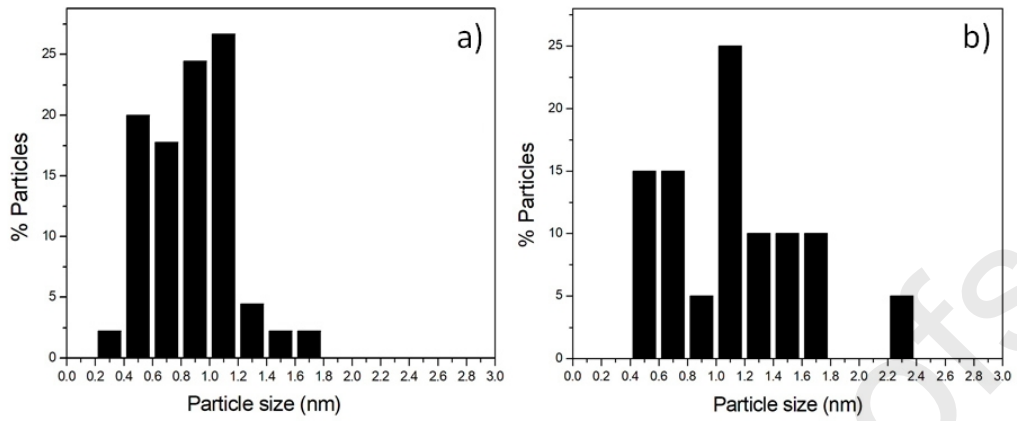

Figure S1. a) Particle size distribution of samples Cu1/CZ showing a mean size of 0.9 nm, a dispersion of 74% after measuring 45 nanoparticles and b) Cu2/CZ with a mean size of 1.1 nm, a dispersion of 60% and 20 nanoparticles measured.

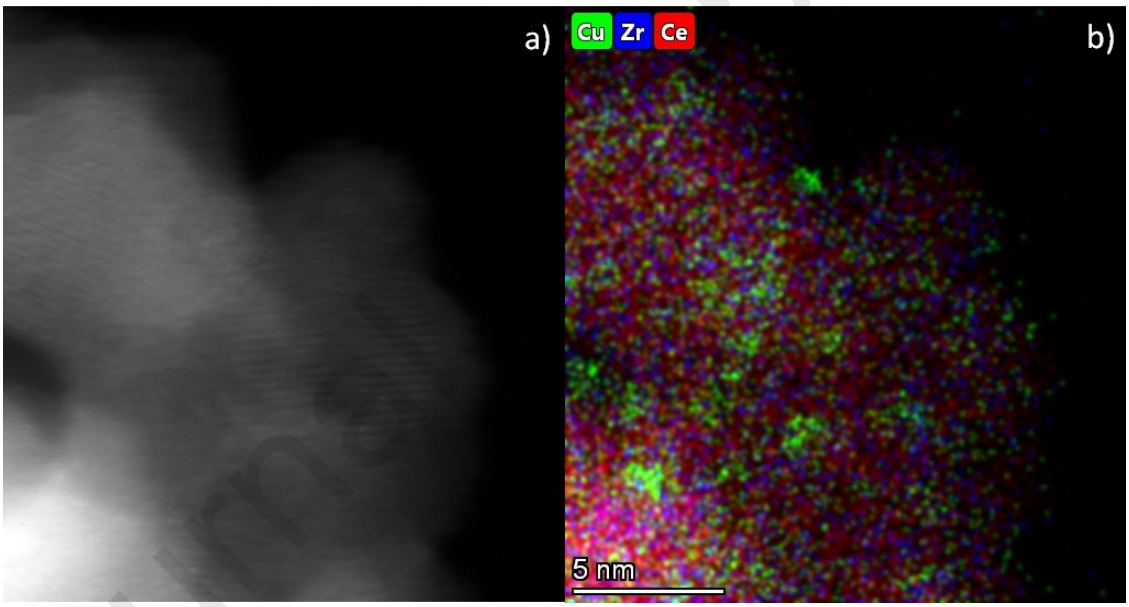

Figure S2. a) HAADF-STEM image together with the corresponding XEDS map b) of an area of the Cu4/CZ sample where small copper particles can be found.

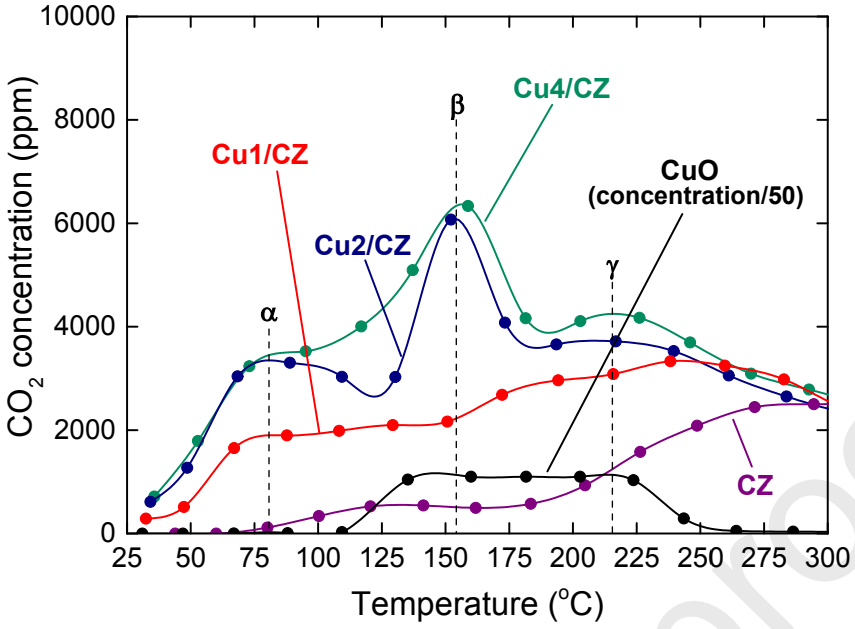

Figure S3. CO oxidation profiles under anaerobic conditions for the catalysts studied (5% CO/He; 35 ml/min; 5°C/min).

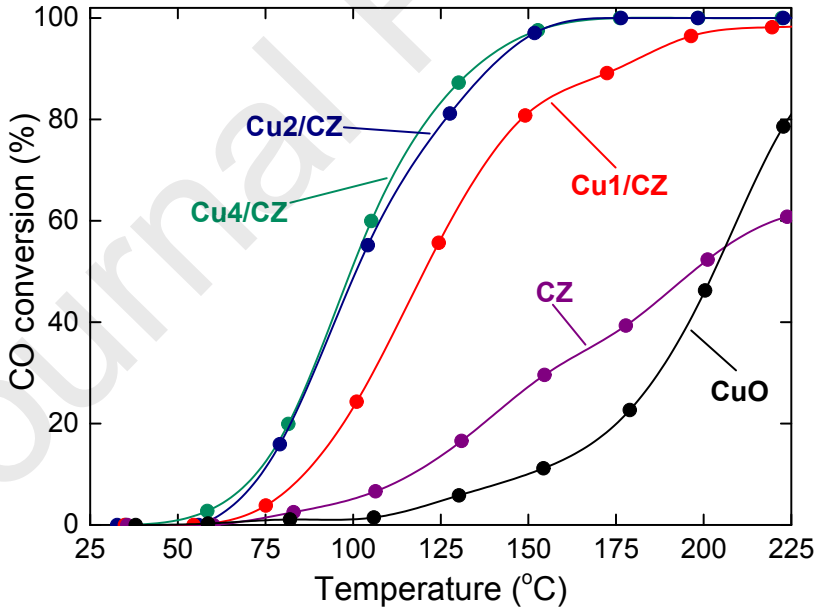

Figure S4. CO oxidation profiles under anaerobic conditions for the catalysts studied (1000 ppm CO/10% O_2/He; 100 ml/min; 5°C/min).

Declaration of interests

☒ The authors declare that they have no known competing financial interests or personal relationships that could have appeared to influence the work reported in this paper.

☐The authors declare the following financial interests/personal relationships which may be considered as potential competing interests: